NUMERICAL SIMULATIONS OF AIRFLOW AND HEAT TRANSFER IN A ROOM WITH A LARGE OPENING

David Park

Thesis submitted to the faculty of the Virginia Polytechnic Institute and State University in partial fulfillment of the requirements for the degree of

Master of Science
In
Mechanical Engineering

Francine Battaglia, Chair
Bahareh Behkam
Scott T. Huxtable

10/9/2013
Blacksburg, VA

Keywords: Natural ventilation, single-sided ventilation, buoyancy-driven flows

Numerical simulations of airflow and heat transfer in a room with a large opening

David Park

ABSTRACT

Natural ventilation is an effective method to save energy required to condition buildings and to improve indoor air quality. Computational fluid dynamics (CFD) was used to model single-sided buoyancy-driven natural ventilation in a single room with a heater and door. The velocity and temperature profiles at the doorway agreed fairly well with published literature that includes Mahajan's experimental [2] and Schaelin et al's numerical studies [1]. The 2D and 3D models predicted the neutral level with a difference of 5.6 % and 0.08 % compared to the experimental results, respectively. Using solutions at the doorway, heat transfer rates were calculated. More realistic situations were studied considering conduction, various ambient conditions, wind speeds, and additional heat sources and furniture in the room. The heat loss through the wall was modeled and the airflow and temperature within the room showed no significant changes despite modeling conduction through the walls. Various ambient temperatures and wind speeds were tested, and the neutral level height and total heat transfer rate through the doorway increased with decreasing ambient temperatures. However, the neutral level did not significantly change as wind speeds varied. Total heat transfer rate at the doorway became positive, that is heat transferred into the room, with wind speed. Lastly, the effect of additional heat sources (mini-refrigerator, monitor and computer) and furniture (bookshelf, desk, chair and box) on airflow and heat transfer in the room was analyzed by comparing with a simple case of a room with a heater. Large velocities and high temperatures were predicted in the vicinity of the heat sources. However, the spatially averaged velocity and temperature did not change significantly despite additional heat sources. The room with

furniture was modeled at lower ambient temperature, where the spatially averaged velocities were larger and temperatures were lower than the simple case. The room heated up and reached its thermal comfort level, but the velocities exceeded the maximum acceptable level set by ASHRAE guidelines [8]. Wind was considered simultaneously with the lower temperature, and the room was cooled faster with wind. However, the room was never able to achieve the comfortable level both in velocity and temperature.

Acknowledgements

Foremost, I thank God for great people who have helped me along my Master study. I thank my advisor Dr. Francine Battaglia, who has supported me continuously and patiently while I adapt into new environment and studies. She learned my strength and weaknesses, and knew how to teach me to improve my skills. I could not have imagined having a better advisor for my study. I also thank Dr. Bahareh Behkam and Dr. Scott Huxtable for serving on my committee.

I thank my parents, Seung-Ryong and Eun-Bok, for all the support and opportunities for me to study in U.S. I know how difficult it is for them to send me to a foreign country and continuously support me through my studies. I could become what I am now because of their sacrifices they took. To my brothers, Sam and Paul, who were always there for my struggles. I thank my host parents, who treated me as one of their own children. I could never thank enough for directing me as parent in U.S while I am in a foreign country. Also to my host brothers and sisters, who became my best friends and family in U.S.

I thank fellow students in CREST lab: Santhip, Lindsey, Bahareh, Jeff, and Michael; It was blessing to have such great people around me in the lab who became good friends and also who helped me through my research and classes.

I thank all my friends, who taught me what great friend means. And last but not least, to Julie. For becoming my best friend and always there to make me a better person.

Table of Contents

List of Figures

List of Tables

Nomenclature

Variables

f	Discretized solution
$\vec{g}$	Gravitational vector
h	Convective heat transfer coefficient
k	Turbulent kinetic energy
p	Order of accuracy
q'	Heat transfer rate per width through the doorway
r	Grid refinement factor
t	Time
$\vec{v}$	Fluid velocity vector $\vec{v} = (u, v, w)$
x	Horizontal coordinate
y	Vertical coordinate
z	Depth coordinate
C_d	Coefficient of discharge
E	Total energy
G	Production of turbulent kinetic energy
H	Height of the doorway
N	Number of cells
P	Pressure
T	Temperature
U	Maximum velocity

Greek Letters

β	Thermal expansion coefficient
ε	Turbulent rate of dissipation
ρ	Density of fluid
μ	Viscosity
$\bar{\bar{\tau}}$	Fluid tensor

Subscripts

1	Fine grid
2	Medium grid
3	Coarse grid
in	Into the room
out	Out of the room
b	Due to buoyancy
k	Due to mean velocity gradients
n	Neutral level
p	Constant pressure
t	Turbulence
w	Wall
wind	Wind
0	Reference
∞	Ambient condition

Superscript

*	Non-dimensional value, given
+	Non-dimensional value based on wind speed, given

Chapter 1: Introduction

1.1 Motivation

Energy consumption is an important issue and has become a great concern during the last few decades. The energy demand has increased at a rate of 2 % per year for the past 25 years and it will continue to rise at the same rate if current energy patterns persist, according to the International Energy Agency (IEA) [3, 4]. Building energy utilization accounts for a large portion of overall energy consumption. Most building energy is used for space heating and cooling purposes, and approximately 51% of energy consumption in residential buildings [5]. One method of saving energy costs required for mechanical ventilation of buildings is the use of natural ventilation, which supplies and removes air to the building without using mechanical systems. Natural ventilation has significant potential to reduce operating costs to condition buildings while maintaining acceptable indoor air quality [6].

When implementing a natural ventilation system, the indoor air quality must be considered. The average person in the U.S. spends more than 90 % of their time in buildings [7]. Thus, it is important to maintain comfortable indoor conditions. The ASHRAE standard 55-2010 [8] recommends the maximum air velocity and temperature to be 0.2 m/s and 25 °C, respectively.

There are two types of natural ventilation: wind-driven ventilation and buoyancy-driven ventilation, and occur by wind and buoyancy forces, respectively. The buoyancy forces are induced from density gradients occurring due to temperature gradients. The airflow and thermal conditions in the building can be altered by heat sources such as fires, electronic components, electrical heaters, and even from people. There are two main ventilation principles: cross and single-sided ventilation. Cross ventilation is usually used for cooling

purposes, which relies on wind to transport the cool air into an inlet (window, door, etc.) and to transport the warm interior air through an outlet. Single-sided ventilation involves a room with one opening. The temperature difference between the indoor and the outdoor environment creates a pressure difference, and the air is ventilated through an opening.

Designing a naturally ventilated building is a greater challenge than designing a mechanically ventilated building because natural ventilation depends on weather, which changes continuously. For a mechanically ventilated building, ambient conditions outside the building are not as important. Without any openings, the room can be maintained at comfortable thermal conditions. However for a naturally ventilated building, fluctuating ambient temperature, humidity, wind speed, and wind direction must be considered. How the changes in weather affect the airflow in the building is the broader research question. The spatial layout of the building also must be considered when designing a naturally ventilated building. The position and geometry of opening, heat sources, or objects (furniture) are important factors that affect the airflow in the building.

There are several approaches to study the principles of natural ventilation, commonly experimental investigation and numerical analysis. Experiments are suited to study realistic airflow patterns, but it is expensive and time consuming. In addition, it is difficult to study the details of the airflow patterns in a building. Another method to model natural ventilation in a building is computational fluid dynamics (CFD), which is a numerical analysis to solve the Navier-Stokes equations and predict the airflow within the building. In contrast to experimental methods, CFD is cost-effective and easy to investigate the effect of changes in geometry on the flow. In addition, CFD provides spatial information giving values for variables throughout the entire flow domain. CFD has great potential to become a powerful

tool to model natural ventilation in buildings with careful and correct modeling of the problem.

1.2 Previous Work

Studies have been performed to understand the physics of natural ventilation systems. Mahajan [2] experimentally measured the heat and mass transfer through an opening, placed between two different thermally-conditioned rooms. The velocity and temperature measurements at the doorway (opening) were compared with values predicted by an algorithm based on the application of Bernoulli's equation. However, the analyses showed that the values from an algorithm did not agree well with the experimental results. Schaelin et al. [1] utilized CFD and validated a model to predict a free plume and single-sided ventilation, modeling the work of Mahajan.

Several studies have been pursued using CFD for natural ventilation through buildings, in addition to Schaelin et al. Gan [9] evaluated the effective depth of fresh air in rooms for single-sided buoyancy-driven ventilation. Cho and Awbi [9] studied the effect of heater locations in a ventilated room and predicted the mean velocity for different locations of the heater. Stoakes et al. [10, 11] modeled natural ventilation flows in large, multistory buildings using the commercial software Fluent 6.0. They performed passive cooling and heating cases in whole buildings, and showed the potential of CFD to model natural ventilation in buildings.

The challenge of CFD is modeling realistic flows, particularly in the area of turbulence modeling and buoyancy driven flow. The most common turbulence model is the k-ε model in which the turbulent kinetic energy, k, and turbulent dissipation rate, ε, are modeled. There are three types of k-ε turbulence models: standard k-ε, renormalization group theory (RNG), and

realizable k-ε. The standard k-ε model is considered as the simplest two-equation turbulence model that solves two transport equations. The RNG model includes an additional term to improve the accuracy in the ε transport equation for rapidly strained flows and for swirling flows. The transport equation for ε is also modified for the realizable k-ε model to satisfy certain mathematical constraints on the Reynolds stresses [12].

Several studies have focused on turbulence models appropriate for natural ventilation. Chow and Li [13] tested four turbulence models to study fire-induced thermal plumes: the standard k-ε, low-Reynolds number (LRN) k-ε, Chen-Kim modified k-ε (CK model) and RNG model. The authors found good agreement with experiments using the standard k-ε model while the other models did not give better agreements. Stavrakakis et al. [14] experimentally and numerically investigated natural cross-ventilation in buildings. Three different turbulence models (standard, RNG, and realizable k-ε models) were tested. All turbulence models showed acceptable agreement with the experimental measurements, but overall differences were smallest for the standard k-ε model. Awbi [15] mentioned that the standard k-ε model is the most used and developed turbulence model, and predicts airflow in buildings fairly well.

1.3 Objectives

In the current study, the commercial software FLUENT 12.1 is employed to model and study air stratification in a room with a large opening (single-sided ventilation) and a heater using the standard k-ε turbulence model. The results of Schaelin et al. [1] are validated using two-dimensional (2D) and three-dimensional (3D) simulations in FLUENT. Appropriate boundary conditions are studied and carefully chosen for a realistic representation. Grid resolution and domain size studies are conducted to determine effective modeling of the

problem. The heat transfer rates are calculated using velocity and temperature profiles at the opening. Furthermore, conduction through the wall is modeled. The intention is to study airflow through a large opening in a more realistic situation. The effect of heat loss through the wall on the solutions at the opening is studied. Multiple heat transfer coefficients are tested as boundary conditions at the outer wall of the room and heat losses through the wall are compared.

As mentioned in section 1.1, the natural ventilation system highly depends on ambient conditions and spatial layout in the buildings. Various ambient temperatures and wind speeds are tested and the changes of airflow patterns, temperature and pressure distributions in the room are analyzed. A more complex situation is modeled, where additional heat sources (computer, monitor and refrigerator) and objects (furniture) are considered.

In Chapter 2, numerical models, solution methods, and boundary conditions are presented. Chapter 3 includes grid resolution study and validation of FLUENT for modeling airflow through a large opening. Chapter 4 examines more realistic situations 2D: consideration of conduction, the effect of ambient conditions and winds, and then different spatial layout. In chapter 5, the conclusions of the current work and recommendations for the future work are discussed.

Chapter 2: Numerical Approach

2.1 Governing Equations

The Navier-Stokes equations represent the fundamental governing equations for fluid flow. The conservation of momentum is commonly referred as the Navier-Stokes equation. Additionally, conservation of mass and energy are used to solve the velocity and temperature fields in buildings.

The conservation of mass equation, also called the continuity equation, is:

$$\frac{\partial \rho}{\partial t} + \nabla \cdot (\rho \vec{v}) = 0 \tag{1}$$

where ρ is the density, t is time and $\vec{v}$ is the velocity vector. Conservation of momentum is given by:

$$\frac{\partial}{\partial t}(\rho \vec{v}) + \nabla \cdot (\rho \vec{v} \vec{v}) = -\nabla p + \nabla(\bar{\bar{\tau}}) + \rho \vec{g} \tag{2}$$

Where p is pressure, $\bar{\bar{\tau}}$ is the fluid stress tensor, and $\vec{g}$ is the gravitational vector. The fluid stress tensor for a Newtonian fluid is given by:

$$\bar{\bar{\tau}} = \mu \left[(\nabla \vec{v} + \nabla \vec{v}^T) - \frac{2}{3} \nabla \cdot \vec{v} I \right] \tag{3}$$

where μ is the dynamic viscosity of the fluid and I is the identity tensor. The last term on the right hand side of Equation (2) represents the buoyancy force. The Boussinesq model is employed to solve buoyancy-driven flows and assumes that density can be treated as a constant except in the buoyancy force term [16]. The approximation is only valid when temperature differences are small so that density variations are very small. Relating changes of density and temperature, the thermal expansion coefficient, β, is defined as:

$$\beta = -\frac{1}{\rho}\left(\frac{\partial \rho}{\partial T}\right)_p \approx -\frac{1}{\rho}\frac{\rho_0 - \rho}{T_0 - T} \tag{4}$$

Subscript 0 represents the reference value. Rearranging Eq. (4), the Boussinesq approximation can be represented as:

$$(\rho_0 - \rho) \approx \rho\beta(T - T_0) \tag{5}$$

The conservation of energy is given by:

$$\frac{\partial}{\partial t}(\rho E) + \nabla \cdot [\vec{v}(\rho E + P)] = \nabla \cdot \mathrm{k_{eff}} \nabla \mathrm{T} + \nabla \cdot \left(\bar{\bar{\tau}}_{eff} \cdot \vec{v}\right) + S_h \tag{6}$$

where E is total energy and k_{eff} represents the effective conductivity, which considers the turbulent thermal conductivity in addition to fluid thermal conductivity. Viscous heating is also included in the conservation of energy, which is the second term on the right hand side of the equation.

2.2 Turbulence Modeling

The standard *k*-*ε* turbulence model was used in this study, which assumes that the flow is fully turbulent and the effects of molecular viscosity are negligible. The turbulent kinetic energy, *k*, and its rate of dissipation, *ε*, in the flow field are calculated from two additional transport equations. The *k*-*ε* transport equations are [17]:

$$\frac{\partial}{\partial t}(\rho k) + \nabla(\rho k u_i) = \nabla\left[\left(\mu + \frac{\mu_t}{\sigma_k}\right)\frac{\partial k}{\partial x_j}\right] + G_k = \nabla\left[\left(\mu + \frac{\mu_t}{\sigma_k}\right)\frac{\partial k}{\partial x_j}\right] + G_k + G_b - \rho\varepsilon \tag{7}$$

$$\frac{\partial}{\partial t}(\rho \varepsilon) + \nabla(\rho \varepsilon u_i) = \nabla\left[\left(\mu + \frac{\mu_t}{\sigma_\varepsilon}\right)\frac{\partial \varepsilon}{\partial x_j}\right] + C_{1\varepsilon}\frac{\varepsilon}{k}(G_k + C_{3\varepsilon}G_b) - C_{2\varepsilon}\rho\frac{\varepsilon^2}{k} \tag{8}$$

In these equations, G_k and G_b are the production of turbulent kinetic energy due to mean velocity gradients and buoyancy respectively. μ_t is the turbulent viscosity. The turbulent kinetic energy productions and turbulent viscosity parameters are expressed as:

$$G_k = \mu_t S^2 \tag{9}$$

$$G_b = -\vec{g}\beta\frac{\mu_t}{\rho \mathrm{Pr}}\nabla T \tag{10}$$

$$\mu_t = \rho C_\mu \frac{k^2}{\varepsilon} \tag{11}$$

where C_μ is a constant with a value of 0.09; $C_{1\varepsilon}$, $C_{2\varepsilon}$, and $C_{3\varepsilon}$ are also constants; σ_k and σ_ε are turbulent Prandtl (*Pr*) numbers for k and ε respectively. The values of these parameters used by FLUENT are: $C_{1\varepsilon}$ = 1.44, $C_{2\varepsilon}$ = 1.92, σ_k = 1.0, and σ_ε = 1.3. $C_{3\varepsilon}$ determines the degree to which ε is affected by the buoyancy. It is not specified in FLUENT, but is calculated using a relationship between the velocity vector parallel and perpendicular to gravitational vector.

2.3 Discretization Methods

The segregated pressure-based Navier-Stokes (PBNS) solver is used. The pressure-based solver employs the projection method, an effective method to numerically solve incompressible fluid-flow problems [18]. In the projection method, conservation of mass is rewritten as pressure that becomes the primitive variable. One of the segregated algorithms, the semi-implicit method for pressure-linked equations (SIMPLE) is chosen to solve pressure-velocity coupling. In the SIMPLE algorithm, the momentum equations are initially solved with guessed pressure field p^*, where p^* is used to solve the velocity field $\vec{v}^*$. The corrections to velocity field and pressure are proposed so that the final velocity field satisfies continuity. The final velocity field and pressure can be expressed as:

$$\vec{v} = \vec{v}^* + \vec{v}' \tag{12}$$

$$p = p^* + p' \tag{13}$$

where $\vec{v}'$ and p' are velocity field correction and pressure correction, respectively. The relationship between the velocity and pressure corrections can be expressed as:

$$\vec{v}' = -\frac{1}{A_P}\sum_l A_l\,\vec{v}_l' - \frac{1}{A_P}\nabla p'|_P \tag{14}$$

where A_P and A_l are coefficients included in the momentum equations. The subscripts *P* and *l* represent an arbitrary velocity node and the neighbor points that appear in the discretized momentum equation. Combining the discretized continuity equation to corrected velocities and Eq.(12) produces the pressure-correction equation:

$$\nabla[\frac{\rho}{A_P}\nabla p']_P = [\nabla(\rho\vec{v}^*)]_P + [\nabla(\rho\vec{v}')]_P \tag{15}$$

At this point, the velocity corrections $\vec{v}'$ are unknown so the second term on the right hand side of Eq.(15) is neglected. The pressure correction is found using Eq. (15), which is then substituted into Eq. (14) to obtain the velocity correction. Once the velocity and pressure correction has been solved, the velocity fields and pressure are updated using Eqs. (12) and (13), respectively [19].

FLUENT uses a finite volume approach for discretization. The transport equations are integrated over a finite volume defined by a grid element and calculates the dependent variables (e.g. $\vec{v}$,T) at the center of each cell. From these cell centered solutions, values at each face are interpolated using an upwind scheme. In the current study, momentum, energy and turbulent kinetic energy and dissipation rates are discretized using second-order upwind, which uses Taylor series expansions of the upstream cell centered-solution about the cell centroid to calculate the solutions at the faces of each cell. For the gradient and pressure spatial discretization, least squares cell based (LSCB) and PRESTO! are applied, respectively. Time is discretized using a first-order implicit method. The Courant-Friedrichs-Levy (CFL) number of 1 is chosen to determine time step size, where the CFL can be expressed as:

$$\mathrm{CFL} = \frac{U\Delta t}{\Delta x} \tag{16}$$

where U is the maximum fluid velocity. The time step size and smallest cell size are expressed as Δt and Δx respectively. The absolute convergence criteria are set as 10^{-5} except for the energy, which is set as 10^{-7}.

2.4 Boundary Conditions

Figure 2. 1 shows the computational domain and interior features including the heater for the 2D representation of the room investigated in Mahajan [2] and Schaelin et al. [1]. Figure 2.2 shows the 3D representation of the room and the size of the computational domain used for the current study. The room is 4.2 m long, 3 m high and 4 m wide. The door is 0.12 m thick, 2.2 m high and 1 m wide. The heater (wall mounted radiator) is placed along the wall opposite the door, and is 0.12 m thick, 0.6 m high and 3 m wide. The thickness of the walls is also 0.12 m. The ambient conditions at the domain boundary are represented by specifying ambient pressure of 1 atm and temperature of 22 °C (additional cases will be discussed for different temperatures). For all cases, the heater radiates 50 °C of heat to the room. Standard wall functions were used and the no-slip velocity boundary condition is applied for the fluid-wall interaction. First, the wall is modeled as adiabatic and later conduction is considered. For the wall material, the density is 2320 kg/m^3, specific heat is 1138 J/kg·K, and thermal conductivity is 0.5 W/m·K. For the conduction considerations, the heat transfer coefficient at the outer wall is specified, varying from 5 to 25 W/m^2·K. The thermal expansion coefficient of the air is based on the mean temperature of the heater and the ambient temperature.

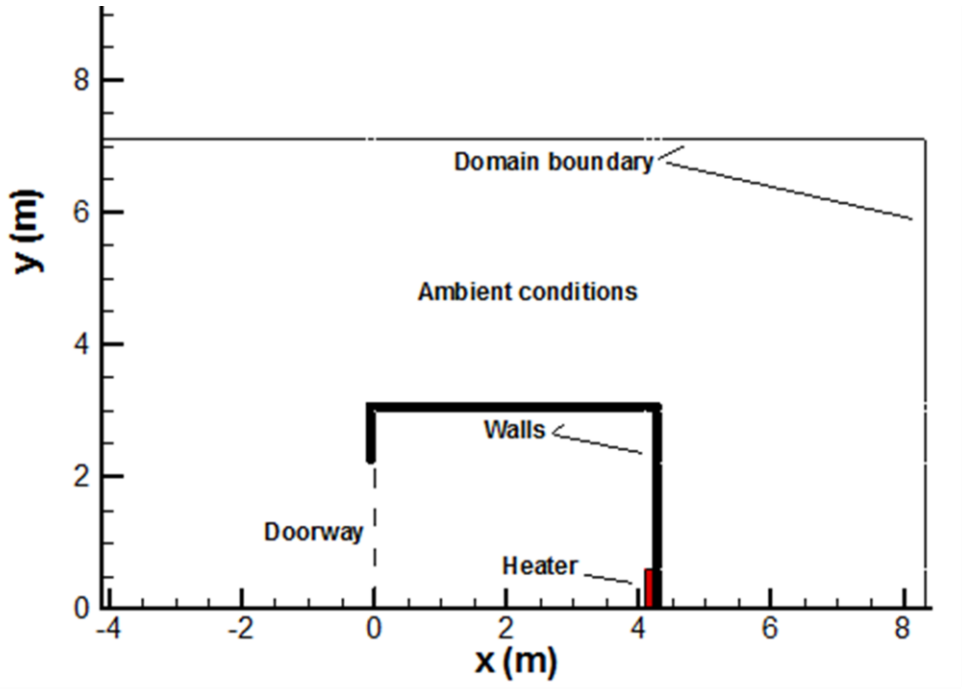

Figure 2. 1 2D view of geometry and conditions for Domain A

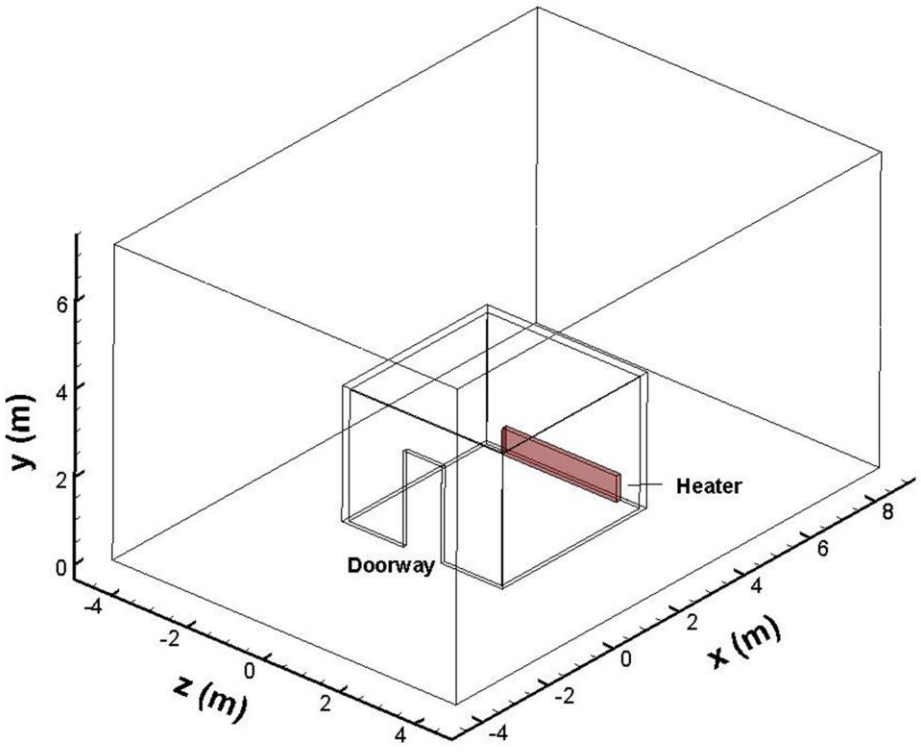

Figure 2.2 3D view of geometry for Domain A

Chapter 3: Airflow and Heat Transfer Through a Large Opening

3.1 Problem Description

Single-sided ventilation is studied and representative velocity and temperature profiles at the doorway are shown in Figure 3.1 (a) and (b), respectively [20]. The neutral level is defined as the point where gage pressure and velocity are zero, and separates the inflow and outflow of the air. Three different sections are visible for the temperature profile at the

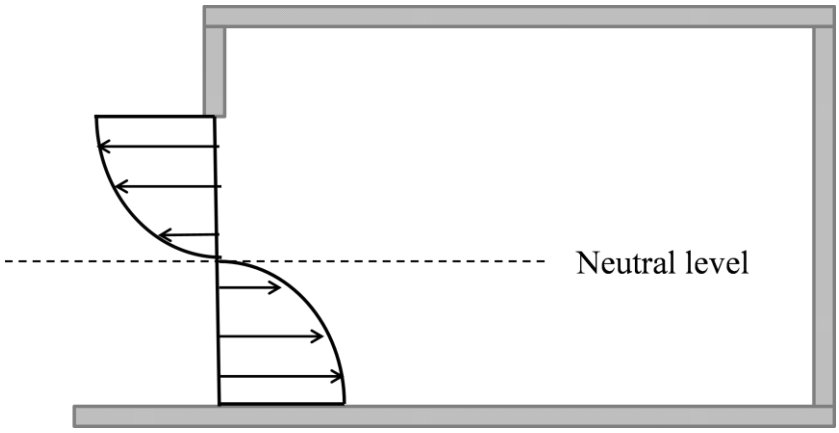

(a) Velocity profile

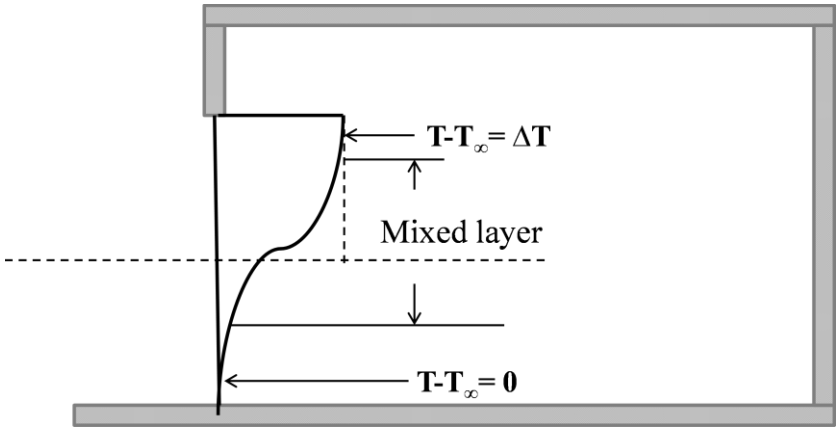

(b) Temperature profile

Figure 3.1 Representative profiles for (a) velocity and (b) temperature in the doorway

doorway: the constant temperature profile ($T=T_\infty$), the mixed layer temperature profile, and the constant temperature profile ($T= T_\infty+\Delta T$). The constant temperature profile below the mixed layer has a value equal to the ambient condition. The mixed layer profile is the section that shows a smooth transition of temperature from ambient temperature to heated air temperature (from the heater); however, the mixed layer does not necessary start at the neutral level.

For the validation studies, the solutions at the doorway for the current modeling are compared to experimental and numerical studies performed by Mahajan [2] and Schaelin et al. [1], respectively. Mahajan performed the experimental work on single-sided ventilation, and measured velocity and temperature at the doorway. Schaelin et al. obtained 2D and 3D simulation results for the single-sided ventilation.

3.2 Grid Resolution Study

The discretization error is studied using the grid convergence index (GCI). The GCI is proposed by Roache [21] for uniform reporting of grid convergence studies. The GCI is based on the Richardson extrapolation [22], where the discrete solutions are assumed to have a series representation of the discretization error. The GCI converts the Richardson extrapolation error estimate into an uncertainty by using absolute values to provide an uncertainty bounds and using a factor of safety F_S. The GCI can be represented as:

$$\mathrm{GCI} = \frac{F_S}{r^p - 1}\left|\frac{f_2 - f_1}{f_1}\right| \tag{17}$$

where r is the grid refinement factor, p is the order of accuracy. Solutions for fine, medium, and coarse grids are subscripted with 1, 2, and 3, respectively. The grid refinement factor r for two-dimensional study is:

$$r = \left(\frac{N_1}{N_2}\right)^{0.5} \tag{18}$$

where N is the number of cells or elements. The order of accuracy is then estimated by using the following equation:

$$p = \frac{\ln\left(\frac{f_3 - f_2}{f_2 - f_1}\right)}{\ln(r)} \tag{19}$$

Two factor of safety values are recommended by Roache for GCI, 3 and 1.25. For grid studies using two grid solutions to determine the observed order of convergence p, $F_S = 3$ is recommended. For three or more grid solutions, $F_S = 1.25$ is adequately conservative.

In the current study, three grid resolutions were compared for uniform grid spacing of 3 cm, 6 cm and 12 cm for fine, medium and coarse grids, respectively. In Figure 3.2, velocity profiles at the doorway are compared with the experimental results from Mahajan [2]. Two adjoining rooms were prepared under two different conditions, one room was cooled to an

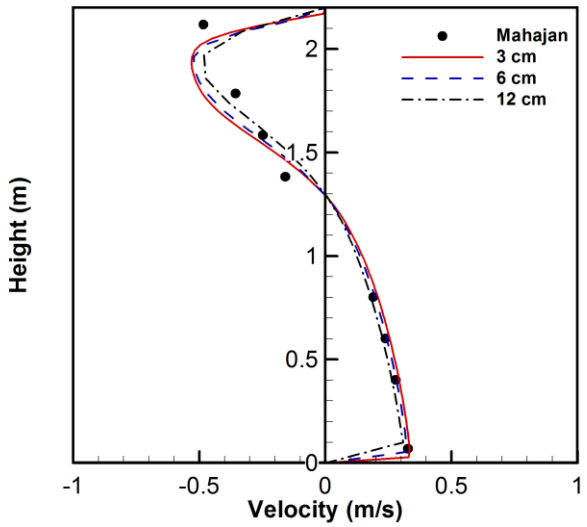

Figure 3.2 Velocity profiles at the doorway for three different grid spacings and compared to Mahajan [2]: Fine (solid), Medium (dashed), and Coarse (dot and dash). Used under fair use, 2013

Table 3.1 Height and velocity predictions for fine, medium and coarse grid

	Fine	Medium	Coarse
Neutral level Height (m)	1.29	1.29	1.30
Peak velocity (m/s) (Above neutral level)	0.33	0.32	0.30
Peak velocity (m/s) (Below neutral level)	-0.53	-0.52	-0.48

average temperature of 19 °C and the other room was heated to an average temperature of 32 °C. The uncertainty of Mahajan's experiment was 0.025 m/s and 0.5 °C in the air speed and temperature measurements, respectively. The magnitude of the peak velocity below the neutral level increased slightly with increasing grid spacing, and is in very good agreement with Mahajan's data. However, the peak velocity above the neutral level deviates from the experimental data due to the uncertainty of the experiment and also difference in representation of ambient condition between the experiment and the simulation. The room temperature was averaged to 19 °C to represent the ambient condition in the experiment, whereas ambient temperature was constant as 22 °C. What is most interesting is that the height of the neutral level remained constant, independent of grid resolution. The predicted peak velocities and the neutral level height are summarized in Table 3.1.

The GCI is calculated using the solutions in Table 3.2 for the neutral level and peak velocities and applying $F_S = 1.25$ and $r = 2$. The GCI for the finer grid, GCI_{21} was relatively low compared to that for the coarser grid, GCI_{32}, showing that the grid refinement was successful. Low values of GCI also indicate that the dependency of the numerical simulation on the cell size has been reduced. The largest GCI_{21} was 3.5% from solutions for peak velocity above the neutral level. The GCI_{21} was less than 0.76% for the two other variables, namely, the neutral level height and peak velocity below the neutral level. As shown in

Figure 3.2 and Table 3.2, the difference between solutions from the fine grid and medium grid was minor.

Dimensionless wall distance for the medium grid was investigated. The law of the wall is based on dimensionless wall distance, y^+ [17]:

$$y^+ = \frac{u_* y_*}{v} \tag{20}$$

where u_* is the friction velocity and v is the kinematic viscosity of the fluid. The near wall node is subscripted with * and y_* is the distance from the wall to the node *. It is recommended by FLUENT [17] that the adjacent wall cell centroid is placed within the log-law layer, $30 < y^+ < 300$. A uniform cell size was used even in the near-wall region and 5 cells are inside the boundary layer near the vertical and horizontal walls. The adjacent wall cell centroid is located between $40 < y^+ < 153$. For the purpose of saving CPU time as well as obtaining accurate numerical solutions, the medium grid resolution is used for the remainder of the study.

3.3 Part 1: 2D modeling

The size of the domain is an important matter, especially for modeling airflow in buildings, because realistic representation of ambient and external airflow is essential. In addition, the size of the domain is another important factor that determines the CPU time. Thus, the study begins with a comparison of the predictions using three different two-dimensional domains. Schaelin et al. [1] used a 2D domain of 34 m × 72.2 m to computationally model the experiments of Mahajan [2]. However, the grid was not very fine having 46 × 46 cells for 2 D.

It is optimal to use small domains that result in accurate numerical solutions and correctly model natural ventilation through buildings. Three domain sizes are modeled using 2D

simulations: Domain A (**오류! 참조 원본을 찾을 수 없습니다.**), and Domain B and C (Figure 3.3). Domain A has the size of 12.44 m × 7.12 m with a grid resolution of 415 × 238 cells. Domain B has the size of 5.44 m x 3.12 m with a grid resolution of 91 × 53 cells.

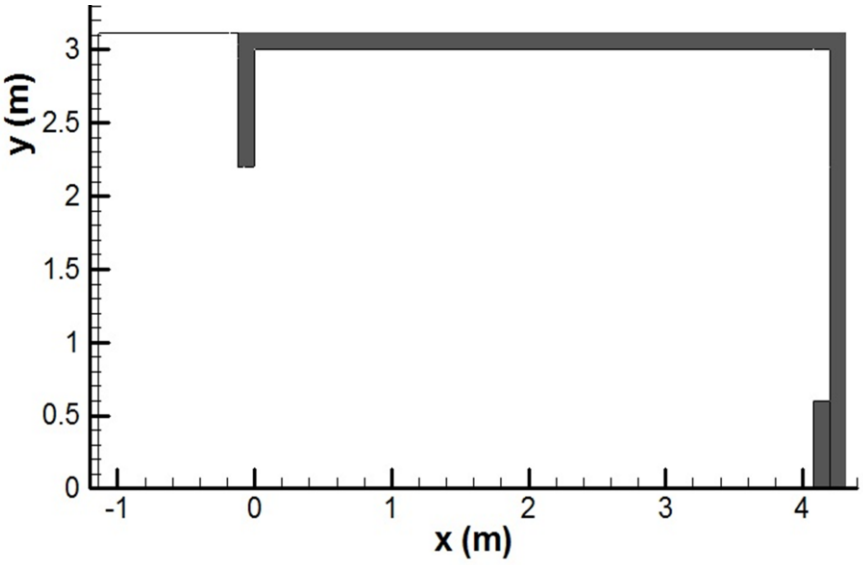

(a) Domain B

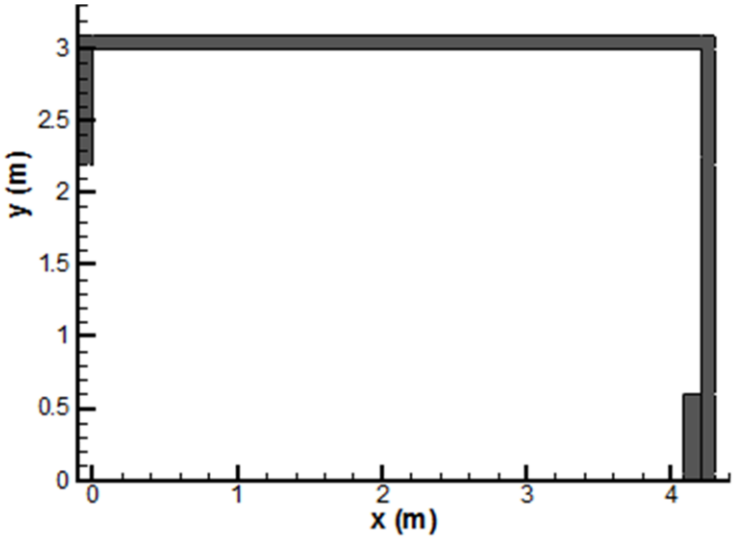

(b) Domain C

Figure 3.3 Domains used for 2D modeling of airflow through a large opening: (a) Domain B and (b) Domain C

Domain C has the size of 4.44 m × 3.12 m with a grid resolution of 74 × 53 cells. The solution becomes quasi-steady (major transient effects have subsided) after 60 s and all data is time averaged from t = 60 – 180 using 3000 time steps.

Non-dimensional velocity and temperature profiles at the doorway are compared by using non-dimensional parameters for height, velocity and temperature:

$$H^* = \frac{2\left(y - \frac{H}{2}\right)}{H} \tag{21}$$

$$u^* = \frac{u}{\sqrt{gH}} \tag{22}$$

$$T^* = \frac{T - T_\infty}{T_w - T_\infty} \tag{23}$$

where H is the height of the doorway, u is x-velocity, and T is temperature. The condition of wall and ambient conditions are subscripted with w and ∞, respectively.

Figure 3.4 (a) and (b) shows non-dimensional velocity and temperature profiles, respectively. The solutions at the doorway from the 2D cases are compared with Mahajan [2]

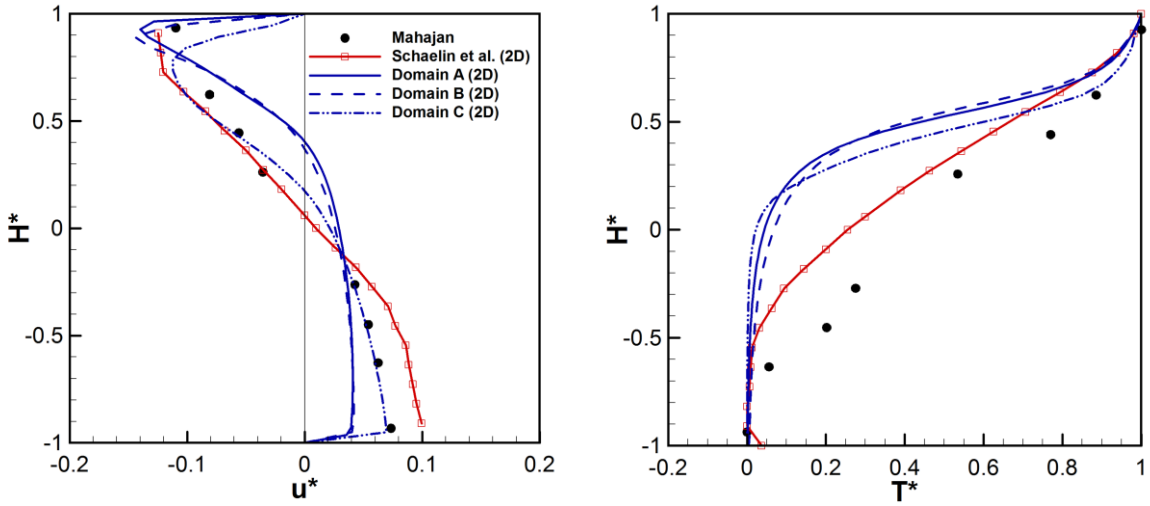

(a) Non-dimensional velocity profile (b) Non-dimensional temperature profile

Figure 3.4 Non-dimensional (a) velocity and (b) temperature profiles at the doorway: Mahajan [2], Schaelin et al. [1] 2D, Domain A, B and C (2D).). Used under fair use, 2013

and Schaelin et al. [1] for their 2D simulation. Neutral level is identified where u^* equals zero. Examining the non-dimensional velocity profiles in Figure 3.4 (a), Schaelin et al. (2D) over-predicted the velocity below the neutral level as compared to Mahajan. Schaelin et al. predicted the neutral level to be approximately 1.21 m, which agrees well with experimental result of Mahajan. The velocity profiles for Domain A (2D) and B (2D) are similar, however, the neutral level is over-predicted by 27 % and 24 % for Domain A and Domain B, respectively. In contrast, the velocity profile for Domain C agrees well with Mahajan's experimental results, and predicts the neutral level with an error of 5.6 %.

In Figure 3.4 (b), the constant temperature profiles are identical below the non-dimensional height of -0.5. The temperature profile for Schaelin et al. (2D) is similar to the data of Mahajan. The temperature profiles for Domains A, B, and C are also similar to each other. However, the current 2D simulations are not consistent with Mahajan or Schaelin et al. (2D), where the starting height of the mixed layer occurs near $H^* = 0$.

The temperature and pressure distributions in the room for Schaelin et al. (2D) and Domain C (2D) are compared in Figure 3.5. The temperature contourlines for the current study are presented in the same fashion as Schaelin et al., where the lines are plotted from 23 °C to 38 °C with an interval of 3 °C and an additional line of 22.5 °C is shown. Pressure lines are plotted from 0 to 1 Pa with an interval of 0.2 Pa and an additional line of -0.5 Pa. The temperature and pressure distributions for Domain C are similar to that for Schaelin et al. (2D). There is evidence of high pressure at both top corners. The zero-pressure line is visible, which separates the inflow and outflow of the air. While the zero-pressure line for Schaelin et al. (2D) remains at the same height across the room from doorway to heater, the height of zero-pressure line slightly decreases for Domain C (2D). The average temperature in the

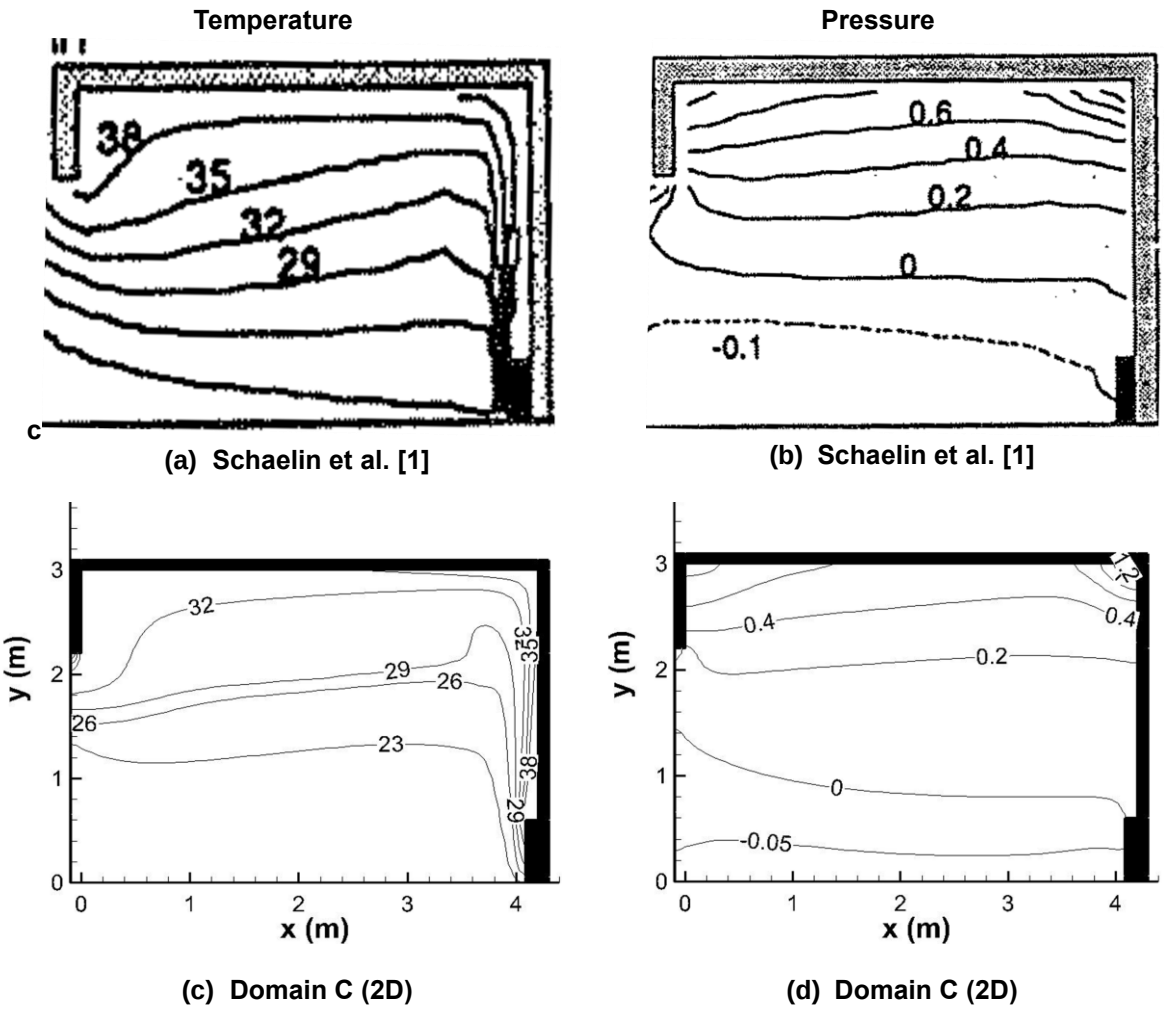

Figure 3.5 Temperature (left) and pressure (right) distributions in the room comparing Schaelin et al. [1] (2D) and Domain C (2D).). Used under fair use, 2013

room is computed to be 26 °C for Domain C, which is the recommended temperature for a building according to ASHRAE guidelines [8].

Velocity vectors and streamlines for Domain C (2D) are shown in Figure 3.6. The velocity is relatively large where the heated air rises from the heater and moves along the right wall and then the ceiling. Looking at streamlines, a circulation zone is present at the top section of the room, between y = 2 m and 2.5 m.

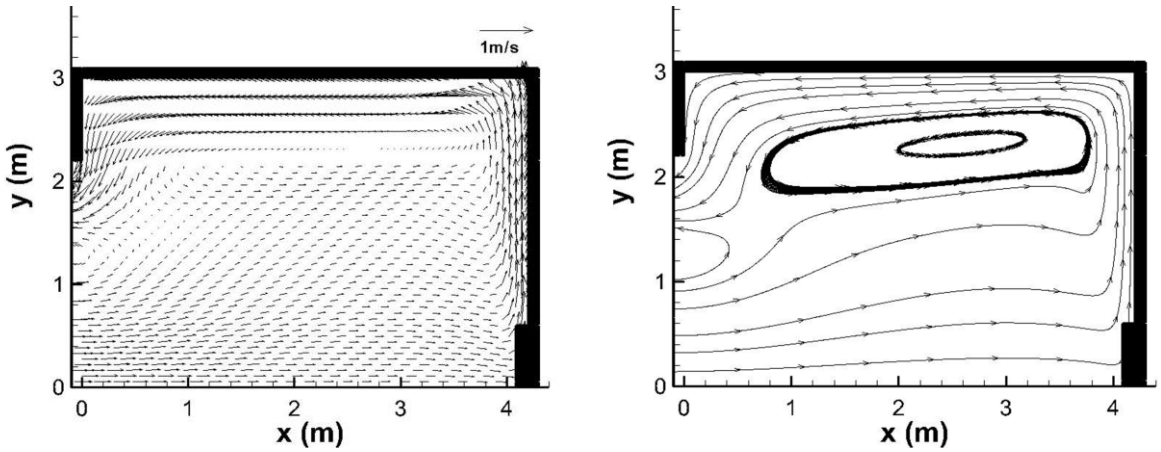

Velocity vectors **Streamlines**

Figure 3.6 Velocity vector (left) and streamlines (right) for Domain C (2D)

3.4 Part 2: 3D modeling

Schaelin et al. [1] used a 3D domain of 34 m × 25 m × 18.7 m, and the grid had 41 × 31 × 31 cells. Two domains are tested for 3D modeling: Domain B (3D) and Domain C (3D). The size of the domain in the *x* - and *y* - directions is the same as the 2D domains (refer to Figure 3.3). The width (z direction) of the domain is 4.24 m. The medium grid (6 cm) cell size is used where Domain B has a grid resolution of 91 × 53 × 71 and Domain C has a grid resolution of 72 × 52 × 71. Domain A is not used for 3D modeling due to grid resolution and CPU constraints. To be consistent with the 2D data, 3D time-averaged data will be presented for $t = 60 – 180$ s using 2400 time steps.

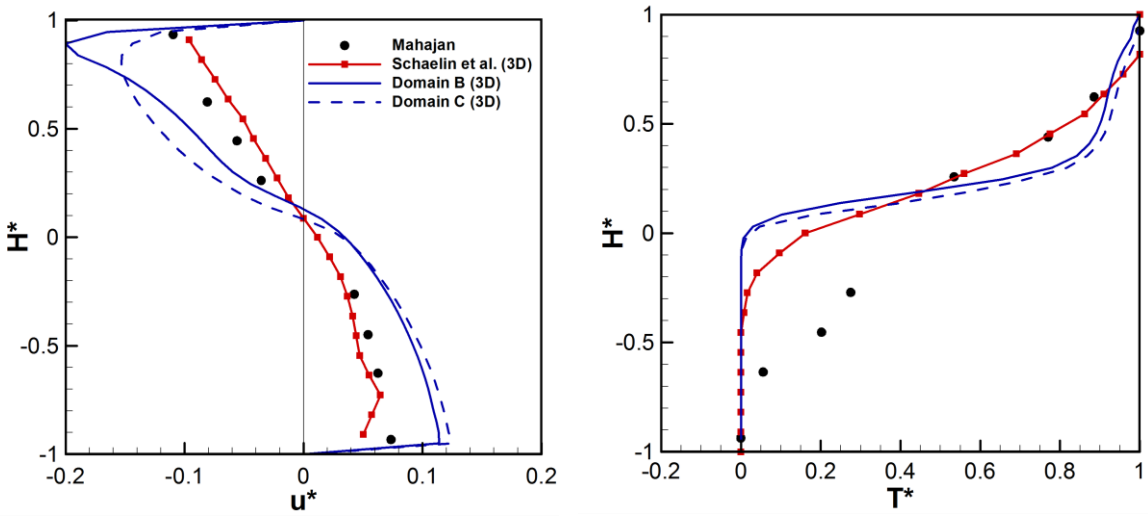

(a) Non-dimensional velocity profile (b) Non-dimensional temperature profile

Figure 3.7 Non-dimensional (a) velocity and (b) temperature profiles at the doorway: Mahajan [2], Schaelin et al. [1] 3D, Domain B (3D) and Domain C (3D).). Used under fair use, 2013

Non-dimensional velocity and temperature profiles from the 3D cases are compared with Mahajan [2] and Schaelin et al. [1] (3D) in Figure 3.7 (a) and (b). Non-dimensional variables are defined the same as in the previous section. The neutral level is better predicted modeling in 3D compared to 2D, where the difference with Mahajan is 2.4 % and 1.5 % for Domain B (3D) and Domain C (3D), respectively. Larger *u*-velocity magnitudes are predicted at the doorway for the current 3D simulations compared to Mahajan. Table 3.2 summaraizes the neutral level predictions for the 2D and 3D simulations.

Table 3.2 Neutral level predictions

	Neutral level(m)
Mahajan	1.21
Schaelin et al. 2D	1.17
Schaelin et al. 3D	1.20
Domain A (2D)	1.54
Domain B (2D)	1.50
Domain C (2D)	1.28
Domain B (3D)	1.24
Domain C (3D)	1.19

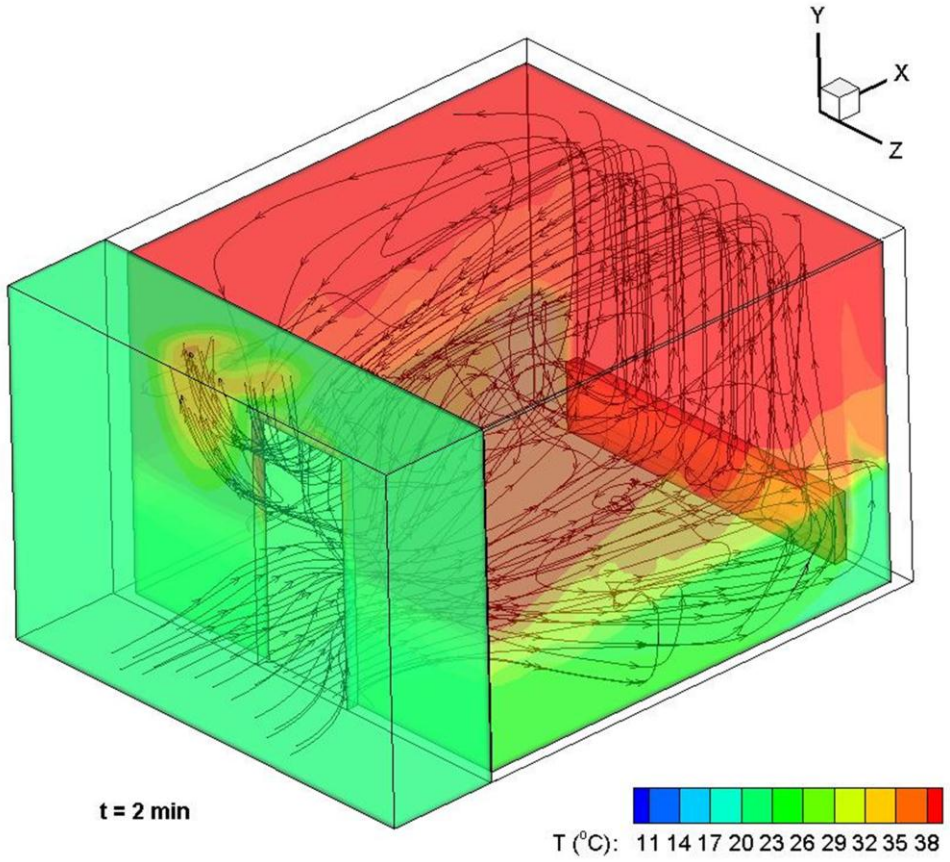

Figure 3.8 Temperature contours with streamlines superimposed in 3D at *t* = 2 minutes for Domain B (3D)

Examining Figure 3.7 (b), the constant temperature profiles before the mixed layer are very similar for the simulations using Domain B and C. The temperature profiles for Domain B (3D) and Domain C (3D) show good consistency with Schaelin et al. (3D), and agree fairly well with the experiment above the non-dimensional height of 0.

Figure 3.8 shows a 3D view of temperature contours with streamlines superimposed for Domain B (3D) after the heater is turned on for 2 minutes. Ambient air enters the room through the bottom of the dooway, which is heated by the heater at the opposite side. Then, the heated air rises and exits through the doorway.

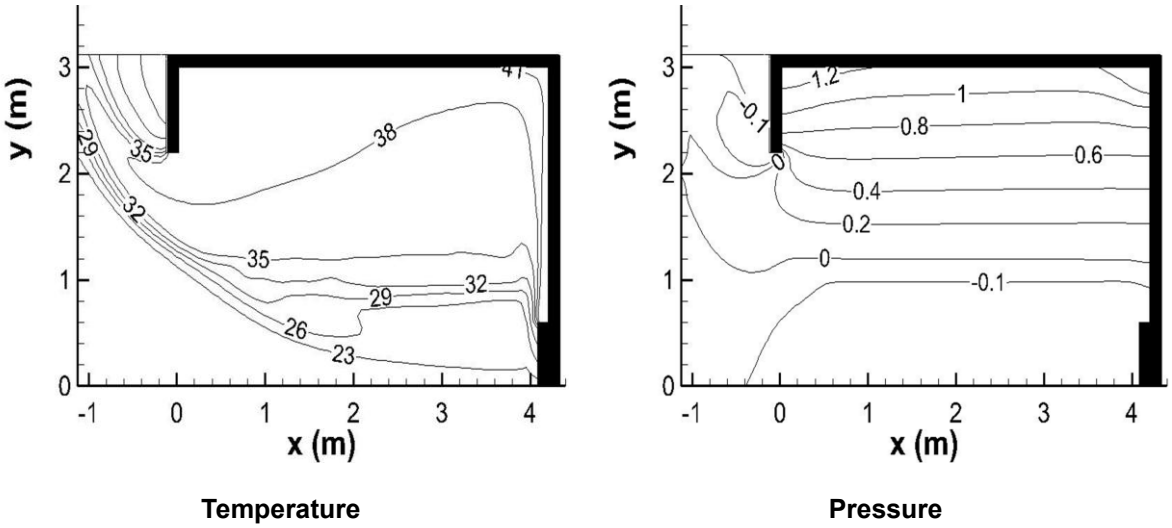

Figure 3.9 Temperature (left) and pressure (right) distributions in the *x–y* plane at z = 0 m for Domain B (3D)

The results are exmined more closely by observing contourlines, vectors and streamlines in the *x*-*y* plane at z = 0 m, which is located at the middle of the door opening. The temperature and pressure distributions for Domain B (3D) at z = 0 m are shown in Figure 3.9 and can be compared to the 2D results of Schaelin et al. [1] shown in Figure 3.5. Similar to the results from Domain C (2D), temperature is high above the heater and at the ceiling. Compared to the 2D simulation (Domain C), 3D simulation (Domain B) predicted higher temperatures in the room, and the pressure contourlines for Domain B (3D) are more evenly distributed, which is consistent with Schaelin et al. (2D). The zero-pressure line also remains at approximately a height of 1 m across the room.

At the same plane, velocity vectors and streamlines are plotted for Domain B (3D) in Figure 3.10. Large velocity is visible along the right wall and the ceiling. Similar to Domain C (2D), one circulation zone develops between x = 2 m and 4 m for Domain B (3D). The circulation zone is smaller in width, but is bigger in height for Domain B (3D) compared to

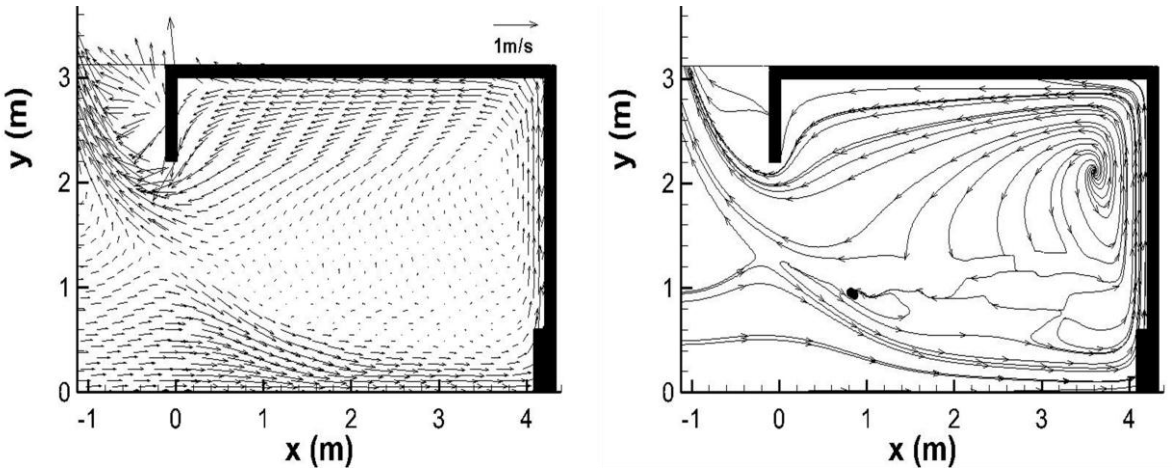

Velocity vectors **Streamlines**

Figure 3.10 Velocity vectors (left) and streamlines (right) in the *x*–*y* plane at *z* = 0 m for Domain B (3D)

Domain C (2D) (refer to Figure 3.6**)**. Airflow in the room is not evenly stratified for the 3D simulation as it is for the 2D simulation. In the next section, heat transfer rates through the opening for all 2D and 3D simulations are presented and compared to heat transfer rates for Mahajan [2] and Schaelin et al. [1].

3.5 Heat transfer through a large opening

Heat transfer rates in a room with a large opening are studied, where for these studies, the opening is a doorway. With an adiabatic wall, the heat transfer only occurs at the door opening. The heat transfer rate at the opening can be calculated by integrating the product of velocity and temperature profiles over the height of the opening. The heat transfer rate per width of the opening (W/m) from ambient conditions to the room can be solved using [23]:

$$q'_{\text{in}} = C_d C_p \int_0^{y_n} \rho_0(y) u(y) T(y) dy \tag{24}$$

where y_n is the neutral level, and C_d is the coefficient of discharge. In the same fashion, heat transfer rate out of the room can be calculated integrating from the neutral level to the height of the opening. Then, the total heat transfer rate is:

$$q'_{\text{total}} = q'_{\text{in}} - q'_{\text{out}} \tag{25}$$

Using the Boussinesq model in FLUENT, density only varies in the buoyancy force, and its value in the domain remains constant. Therefore, the constant value of 1.13 kg/m^3 is used for density. A value of 0.7 is used for discharge coefficient as recommended by Schaelin et al [1].

Heat transfer rates are shown in Table 3.3. Different heat transfer rates are calculated for Schaelin et al. 2D and 3D due to difference in magnitude of the velocity and temperature profiles. The q'_{in} and q'_{out} for Schaelin et al. (2D) are much higher compared to Mahajan [2]. The q'_{in} for Schaelin et al. (3D) is consistent with Mahajan, but the q'_{out} is lower.

The heat transfer rates for Domain A (2D) are similar to Schaelin et al. (3D), but the q'_{total} is positive meaning heat is transferring into the room. Thus, Domain A (2D) predicts a relatively bigger q'_{in} compared to q'_{out}. The q'_{in} and q'_{out} for Domain B (2D) are relatively bigger than those for Domain A (2D) and are between the values for Schaelin et al. 2D and 3D. The lower neutral level predicted using Domain B (2D) results in negative q'_{total} with a magnitude of 0.5 kW/m. The q'_{out} for Domain C (2D) is in very good agreement with Mahajan, but the q'_{in} is slightly higher. With better prediction for the neutral level, q'_{total} is negative. The q'_{total} for Domain C (2D) is -3.8 kW/m, which is in good agreement with Schaelin et al. (3D). The heat transfer rates are much higher for the 3D cases compared to the 2D cases because the velocity magnitudes at the doorway are larger (refer to Figure 3.4 (a) and Figure 3.7 (a)). Both 3D cases result in negative q'_{total} with better prediction in neutral level. Comparing the 3D cases, q'_{total} for Domain C (3D) is bigger than q'_{total} for Domain B

Table 3.3 Heat transfer rates per width of the opening

	q'_{in} *(kW/m)*	q'_{out} *(kW/m)*	q'_{total} *(kW/m)*
Mahajan	55.2	66.2	-11.0
Schaelin et al. 2D	81.4	83.3	-1.9
Schaelin et al. 3D	50.3	53.4	-3.0
Domain A (2D)	54.0	53.6	0.4
Domain B (2D)	71.8	72.3	-0.5
Domain C (2D)	62.1	66.5	-3.8
Domain B (3D)	103.7	115.6	-8.3
Domain C (3D)	108.8	122.9	-14.0

(3D). The neutral level is under-predicted by 1.5 % for Domain C (3D), and thus Domain C (3D) predicts a relatively bigger q'_{out} compared to q'_{in}.

In summary, 2D and 3D simulations were performed using various domain sizes to determine a reasonable geometry for further detailed studies. The neutral level for Domain C (2D) was most consistent with Mahajan among the 2D simulations, having an error of 5.6. In addition, the velocity profile for Domain C (2D) was most consistent with the experiment (Figure 3.4 (a)). The neutral level was better predicted modeling in 3D compared to 2D, where the difference with Mahajan was less than 2.4 % for 3D simulations. Velocity magnitudes were larger compared to the experiment, but temperature profiles for 3D simulations showed good agreement with Schaelin et al. (3D). For the remaining studies, Domain C (2D) will be used for conduction and ambient temperature studies to save CPU time. Domain B (2D) will be considered for simple wind studies to include the effect of doorway for wind and also to have relatively small CPU time compared to Domain A (2D). In addition, Domain B (3D) will be used to model additional heat sources and furniture in the room since Domain B (3D) includes an additional ambient environment.

Chapter 4: Consideration of More Realistic Situations

4.1 Problem Descriptions

The airflow and heat transfer through a large opening were modeled in Chapter 3 using an adiabatic wall boundary condition. In this chapter, more realistic situations are considered and begin with modeling conduction through walls. The effect of conduction through a wall is studied using Domain C (2D) to reduce CPU time. Then, the effect of ambient conditions for representation of cooler days and the effect of wind for representation of windy days are studied. Domain C (2D) is again utilized for the studies. Lastly, more complex spatial layout of the room is considered using Domain B (3D). The details of various boundary conditions and geometry are specified in each section.

4.2 Non-Adiabatic Walls in 2D

In reality, there is always heat transfer occurring through walls of a building. In this section, the main interest is how airflow in the room alters when conduction is considered. The ambient temperature for the convective boundary condition at the outer wall is set as 22 °C. Convective heat transfer coefficients ranging from h = 5 to 25 W/m^2·K in increments of 5 are tested.

The overall solutions did not significantly change as conduction was considered. The sum of the heat transfer rates through the doorway and the walls are equal to q'_{total} for the adiabatic wall. The heat loss through the wall is approximately 4.2% of the total heat transfer rate for h = 5 W/m^2·K, and increases up to 5.6% of the total heat loss with h = 25 W/m^2·K. Figure 4.1 shows the heat loss through walls with respect to h. As expected, heat loss through the walls increase with increasing h. In addition, it shows that the change in heat loss through the walls becomes trivial for higher values of h, representative of very windy days.

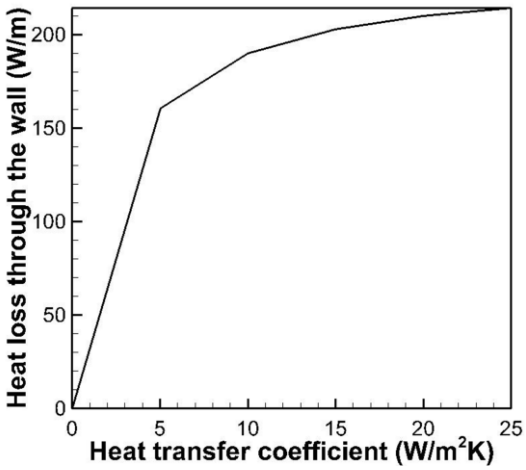

Figure 4.1 Changes in heat losses through wall with respect to convective heat transfer coefficients

The temperature contours for an adiabatic and a non-adiabatic wall with h = 5 W/m$^{2.}$K are shown in Figure 4.2. Only the results from the case with h = 5 W/m^{2}K are presented because changing h did not significantly affect the results. The temperature gradients occur in the wall (Figure 4.2 (b)); however, the overall temperature distribution within the room has not changed much considering conduction through wall. The velocity and temperature profiles at the doorway (x = 0 m) and at the center of the room (x = 2 m) are compared in Figure 4.3 (a) and (b), respectively. The velocity profiles for both adiabatic and non-adiabatic wall conditions are identical (Figure 4.3 (a)). At the top of the doorway (y = 2.2 m), the peak temperature reduced by 1 °C due to heat loss through the wall. The temperature profile at the center of the room shows minor differences when comparing the adiabatic and non-adiabatic wall conditions. Temperature gradients are linear at the height between 3 to 3.12 m for the non-adiabatic wall, where the section represents conduction through the wall, and demonstrates that conduction was correctly modeled. Overall, it can be stated that the flow field in the room is not affected significantly by the heat loss through the wall.

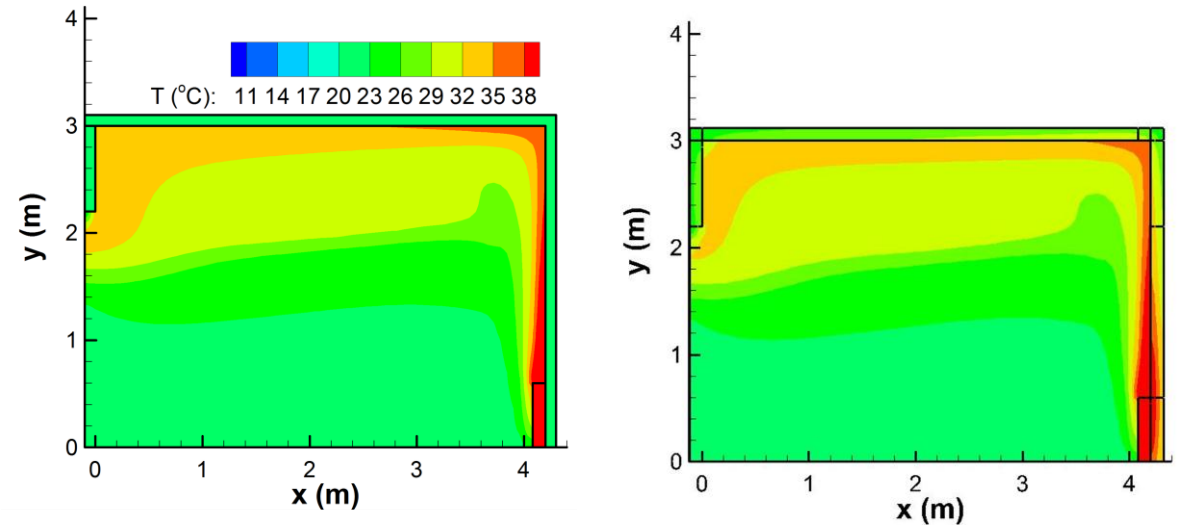

(a) Adiabatic wall (b) Non-Adiabatic wall

Figure 4.2 Temperature contours for (a) adiabatic wall and (b) non-adiabatic wall

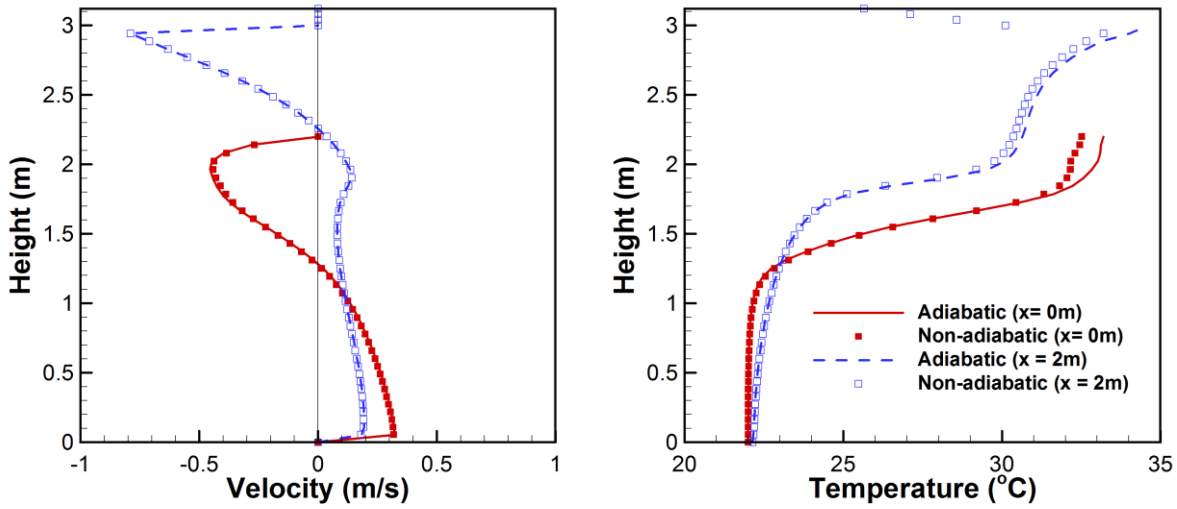

(a) Velocity profile (b) Temperature profile

Figure 4.3 (a) Velocity and (b) temperature profiles at *x* = 0 m (opening) and at *x* = 2 m (center of the room) for cases with adiabatic and non-adiabatic wall

4.3 The effect of ambient temperature

The effect of ambient temperature is studied for the non-adiabatic wall using h = 5 W/m^2·K, and T_∞ = 22 °C, 18 °C and 14 °C. The non-dimensional velocity and temperature profiles at the doorway are compared in Figure 4.4 (a) and (b). The peak velocity flowing out of the room decreases as the ambient temperature decreases, while the neutral level height increases. The peak velocity flowing into the room is largest for T_∞ = 22 °C. Interestingly for T_∞ = 14 °C, the velocity profile indicates that air is moving out of the room near the floor. The non-dimensional temperature profiles are very similar for various ambient temperatures (Figure 4.4 (b)). The constant temperature section is captured for each case, and the starting height of the mixed layer is approximately the same.

Using the velocity and temperature profiles, the heat transfer rates at the doorway are calculated and summarized in Table 4.1. As the ambient temperature decreases from 22 °C to

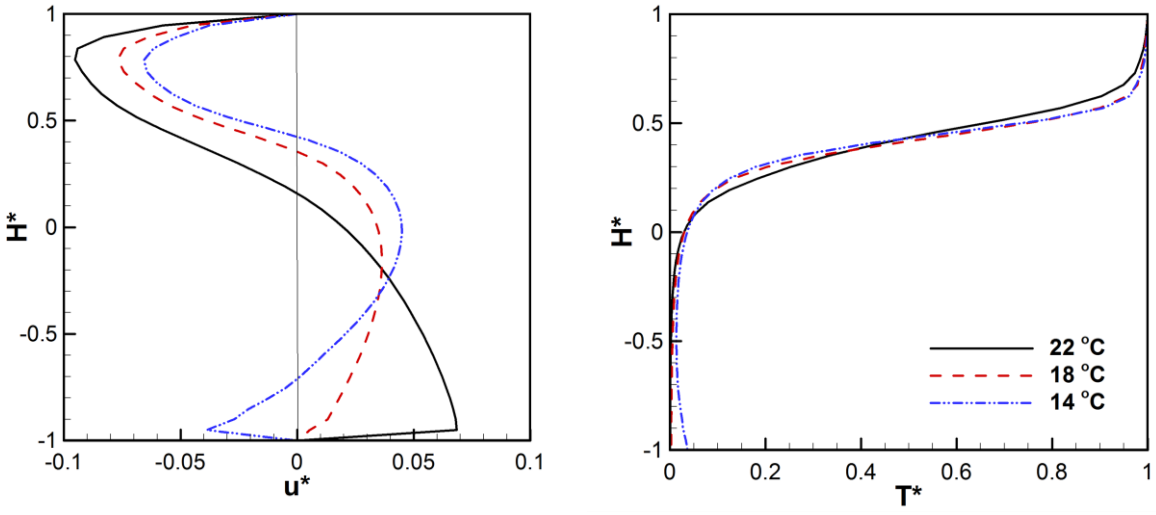

(a) Non-dimensional velocity profile **(b) Non-dimensional temperature profile**

Figure 4.4 (a) Velocity and (b) temperature profiles at *x* = 0 m (opening) for different ambient temperature: 22 °C (solid), 18 °C (dashed) and 14 °C (dash and a dot)

Table 4.1 Heat transfer rates at the doorway calculated for three ambient temperatures (T_∞ = 22, 18, and 14 °C)

T_∞	q'_{in} (kW/m)	q'_{out} (kW/m)	q'_{total} (kW/m)
22 °C	61.6	65.3	-3.6
18 °C	41.5	40.3	+1.2
14 °C	40.2	37.8	+2.4

18 °C, q'_{in} and q'_{out} reduces by 32% and 38% respectively. As ambient temperature changes from 18 to 14 °C, the change in q'_{in} and q'_{out} is not as significant relative to T_∞ = 22 °C. The total heat transfer rate at the doorway is 1.2 and 2.4 kW/m for the ambient temperatures of 14 °C and 18 °C, respectively. The q'_{total} is positive due to a larger reduction in q'_{out} when T_∞ is reduced from 22 °C to 14 °C .

Figure 4.5 shows the temperature contours with velocity vectors. For higher ambient temperature, the temperature in the room is more evenly distributed. The average temperature in the room is 26 ℃, 25 ℃ and 23.7 ℃, for T_∞ = 22 ℃, 18 ℃, and 14 ℃, respectively. Heated air rises along the right wall, and moves toward the doorway along the ceiling.

Pressure contours with streamlines are shown in Figure 4.6. The highest pressure occurs at the top corner above the heater, and then at the opposite top corner. As ambient temperature decreases, the negative pressure zone moves to the middle section of the room, and the lowest pressure is visible at x = 1 m and middle of the opening for ambient temperature of 14 ℃. The circulation zone develops at a height of 2 m, where it increases in size with decreasing ambient temperature. The velocity profile at the doorway in Figure 4.4 shows negative velocity at the bottom section of the opening for ambient temperature of 14 ℃. At the bottom section of the doorway for 14 ℃, the ambient air enters the room to x = 0.5 m and then circulates out of the room.

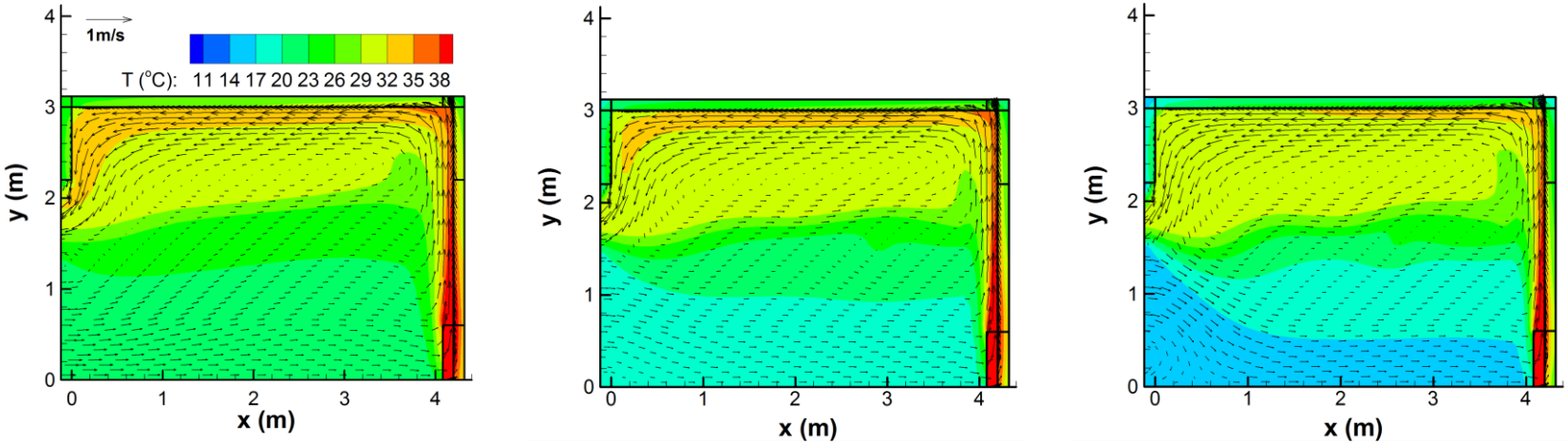

(a) 22 °C (b) 18 °C (c) 14 °C

Figure 4.5 Temperature contours with velocity vectors for various ambient temperatures: (a) 22 °C, (b) 18 °C and (c) 14 °C

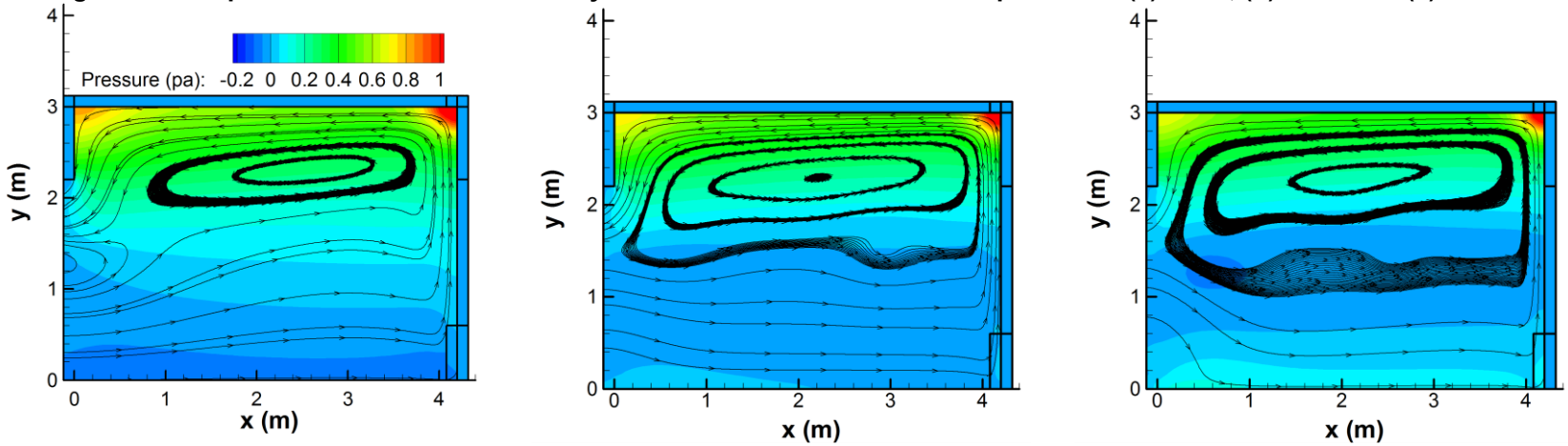

(a) 22 °C (b) 18 °C (c) 14 °C

Figure 4.6 Pressure contours with streamlines for various ambient temperatures: (a) 22 °C, (b) 18 °C and (c) 14 °C

4.4 The effect of wind speed

In this section, wind-driven ventilation is studied in addition to buoyancy-driven ventilation. The study focuses on how air conditions in the room alter with wind spped. Three different velocities are tested: 1 m/s, 5 m/s and 10 m/s. Domain B (2D) is shown in Figure 3.3 (a), where the left surface of the domain is set as velocity-inlet for wind boundary conditions. The walls are adiabatic and specified as no-slip surfaces. The ambient temperature is 22 ℃ and the heater is 50 ℃.

Dimensional and non-dimensional velocity profiles at the doorway for three wind speeds and the no wind case are shown in Figure 4.7 (a) and (b), respectively. Dimensional and non-dimensional temperature profiles are shown in Figure 4.7 (c) and (d), respectively. A superscript + represents the non-dimensional quantity based on wind speed, and the new non-dimensional velocity is defined as:

$$u^{+} = \frac{u}{u_{wind}} \tag{26}$$

where u is the *x*-velocity and u_{wind} is wind speed. The result from the no-wind case is not shown in Figure 4.7 (b) since u_{wind} = 0. As expected, peak velocity both above and below the neutral level increases as wind speed increases, however, the non-dimensional velocity profiles collapse for the three wind cases. The height of the constant temperature profiles, when T = T_{∞}, increases as wind speed increases. In addition, the peak temperatures at the doorway decrease with increasing wind speed.

The maximum and minimum velocity and pressure in the room are summarized in Table 4.2. The heat transfer rates at the doorway are calculated for each case as well. As expected, the absolute values of maximum and minimum velocity increase as wind speed increases. The pressure also increases significantly as wind speed changes from 1 m/s to 10 m/s. For the no wind case, q'_{total} is negative meaning that heat is transferring out of the room. In contrast,

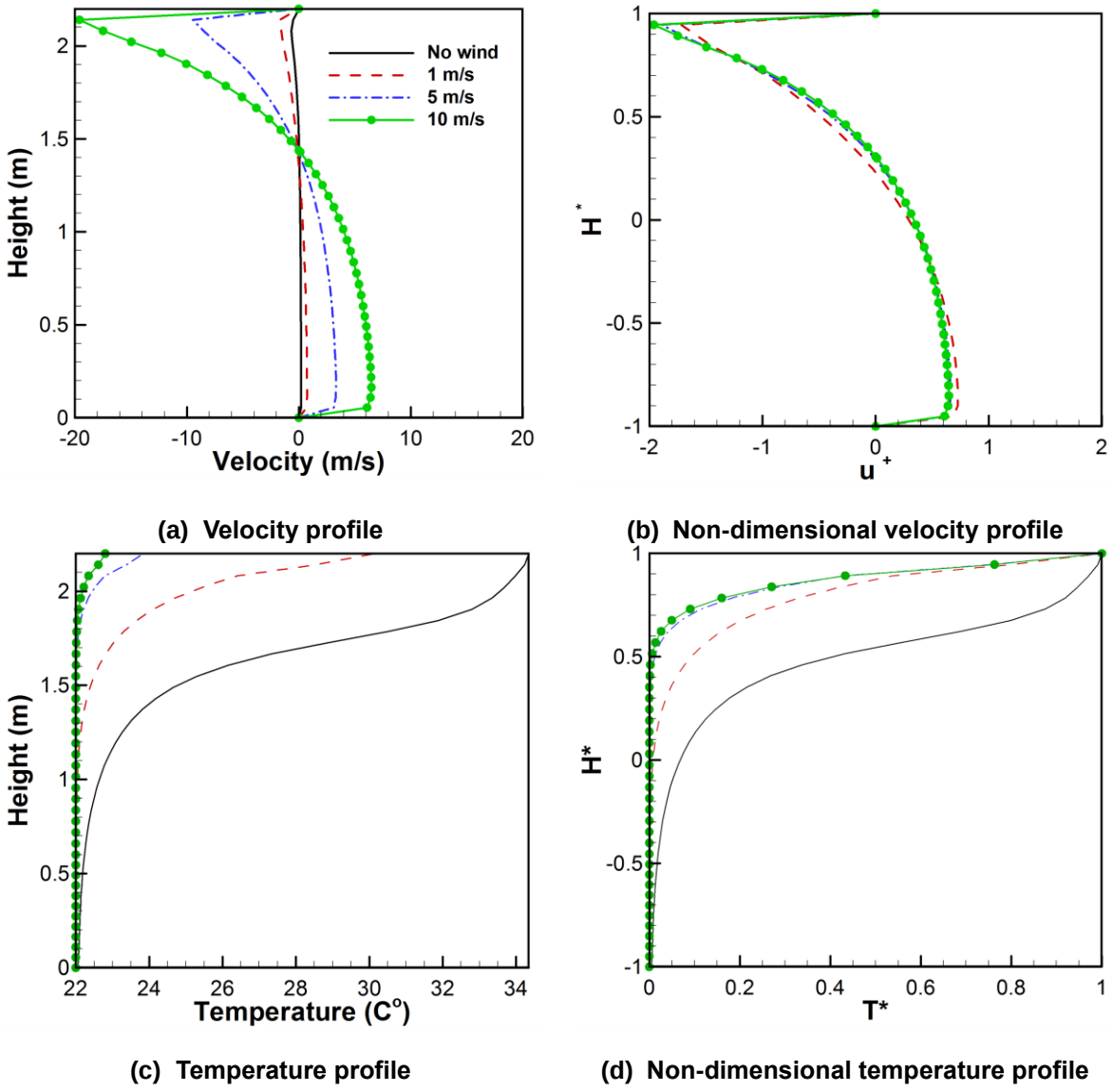

(a) Velocity profile

(b) Non-dimensional velocity profile

(c) Temperature profile

(d) Non-dimensional temperature profile

Figure 4.7 Solutions at the doorway for no wind, 1m/s, 5 m/s and 10 m/s: (a) velocity profile, (b) non-dimensional velocity profile, (c) temperature profile and (d) non-dimensional temperature profile

Table 4.2 Maximum and minimum velocity and pressure in the room, and heat transfer rates at the doorway for No wind, 1 m/s, 5 m/s, and 10 m/s

	No wind	1 m/s	5 m/s	10 m/s
Maximum velocity (m/s)	1.2	4.3	21.3	43.3
Minimum velocity (m/s)	-1.0	-2.5	-13.7	-28.2
Maximum pressure (Pa)	1.2	15.9	319.2	1263.4
Minimum pressure (Pa)	-0.8	-1.9	-114.1	-509.5
q'_{in} ***(kW/m)***	71.8	228.6	1119.0	2204.0
q'_{out} ***(kW/m)***	72.3	214.6	1038.9	2037.4
q'_{total} ***(kW/m)***	-0.50	14.0	80.1	166.6

q'_{total} for the wind cases are positive and increases in magnitude as wind speed increases. It can be concluded that the heat transfer into the room increases at a faster rate than heat transfer from the room with increasing wind speed.

Non-dimensional pressure, x-velocity and y-velocity contours for the wind cases are compared in Figure 4.8 (a), (b), and (c), respectively. Non-dimensional pressure is obtained by dividing pressure by dynamic pressure based on wind speed and y-velocity is non-dimensionalized dividing by wind speed:

$$p^+ = \frac{p}{\frac{1}{2}\rho u_{wind}^2} \tag{27}$$

$$\vec{v}^+ = \frac{\vec{v}}{u_{wind}} \tag{28}$$

where ρ is density of air and $\vec{v}$ is velocity vector $(u,\ v)$. The p^+ contours show that p^+ decreases with increasing wind speed, where p^+ is highest for the wind speed of 1 m/s. In other words, dynamic pressure becomes relatively bigger compared to static pressure with increasing wind speeds.

The u^+ contours are similar at the doorway, where the ambient air enters the room through the bottom section of the doorway (positive u^+), and the heated air exits the room

through the top section of the doorway (negative u^+). The maximum u^+ increases for the faster wind speeds meaning that the ratio of air flowing out to air flowing into the room increases with increasing wind speeds. A region of negative horizontal flow (u^+) near the ceiling is visible for 1 m/s, which diminishes for 5 m/s and 10 m/s.

Examining Figure 4.8 (c), similar v^+ contours are noticeable for 5 m/s and 10 m/s. At the middle of the room, approximately at *x* = 2.5 m, negative vertical flow occurs from ceiling to floor for 5 m/s and 10 m/s. Negative v^+ occurs at the top of the doorway, where its magnitude decreases with increasing wind speed.

Temperature contours with streamlines superimposed for the no wind case and three wind cases are shown in Figure 4.9. A circulation zone develops at the top of the room for the no wind case. As 1 m/s of wind blows into the room, the circulation zone shrinks in size. Three circulation zones are formed for 5 m/s at the right upper corner, the center bottom and the top left corner of the room. Similarly for 10 m/s, three circulation zones develop. Two circulation zones occupy approximately the whole room from x = 1 m to the heater. Temperature contours for no wind and 1 m/s are similar, where heated air rises above the heater and moves toward the doorway along the ceiling. Interestingly, heated air is more distributed around the room for u_{wind} = 5 m/s and 10 m/s due to large circulation zones.

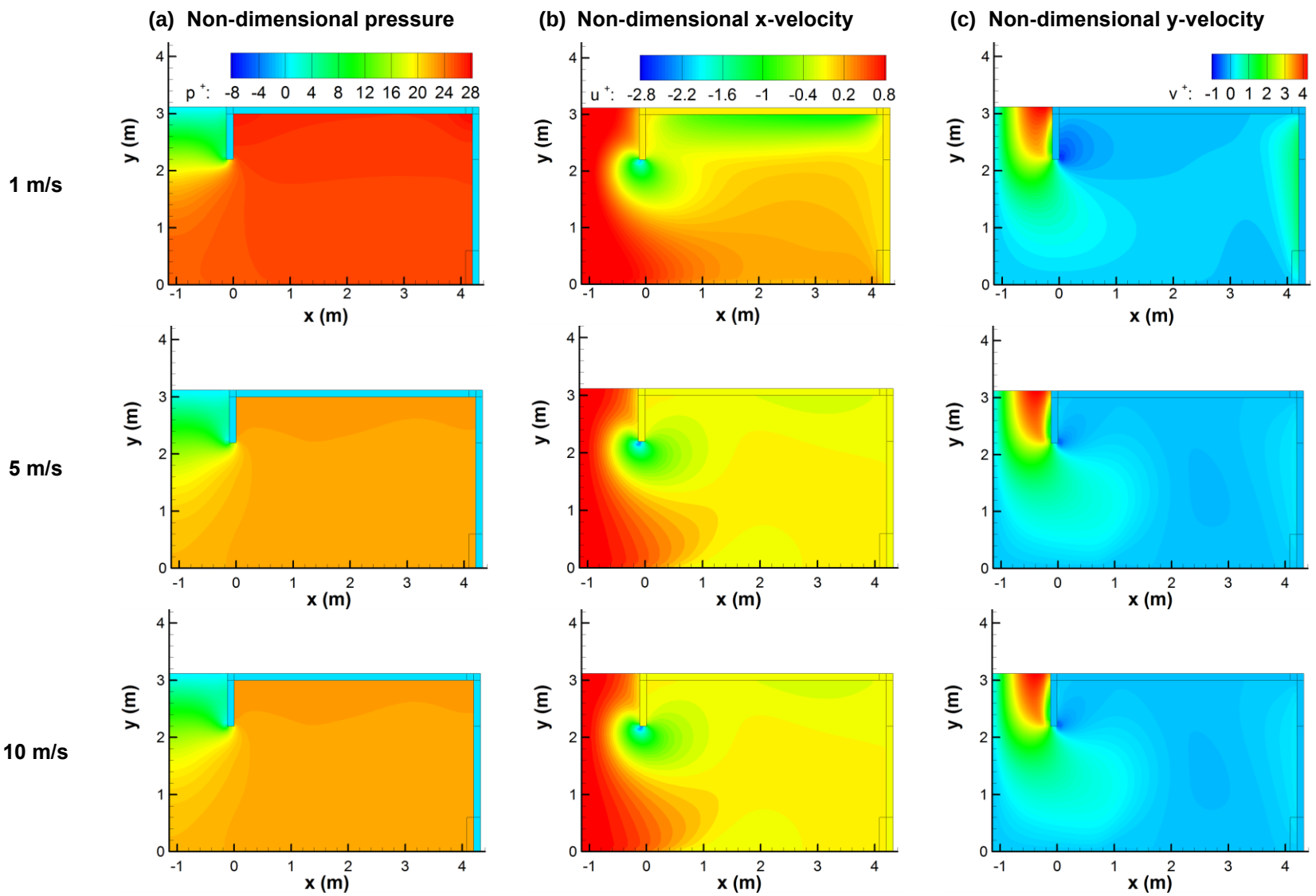

Figure 4.8 Contours for wind speed of 1, 5 and 10 m/s: (a) Non-dimensional pressure, (b) Non-dimensional *x*-velocity and (c) Non-dimensional *y*-velocity

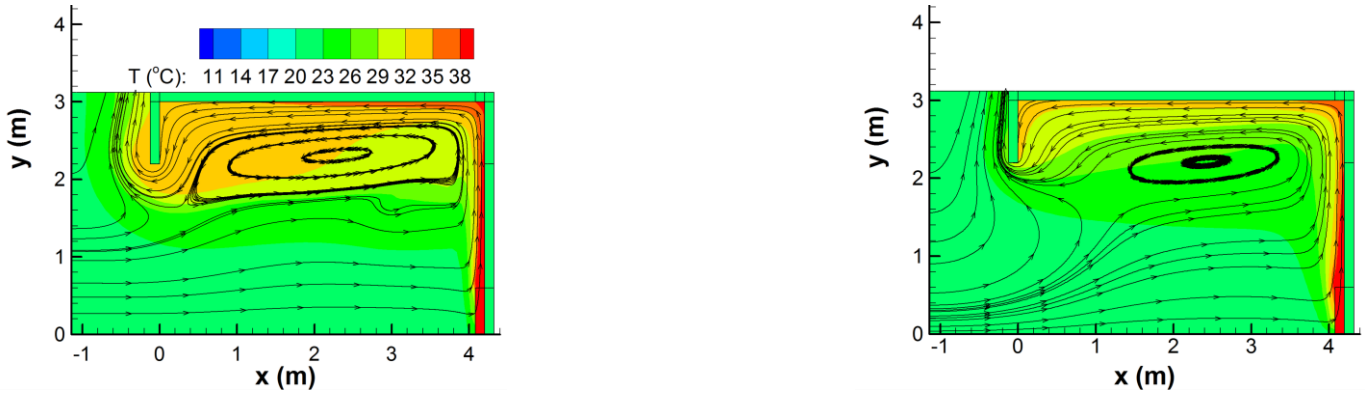

(a) No wind

(b) 1 m/s

(c) 5 m/s

(d) 10 m/s

Figure 4.9 Temperature contours with streamlines: (a) no wind, (b) 1m/s, (c) 5 m/s and (d) 10 m/s

4.5 Additional Furniture in a room

In a realistic room, there is more than just a heater. In this section, additional furniture and heat sources are modeled, where the layout in the room is shown in Figure 4.10. A desk is placed in front of the heater, which has dimensions 0.7 m × 0.65 m × 1.6 m in *x*, *y*, and *z*, respectively. The desk legs are 0.05 m thick in *x*- and *z*- directions. The chair has dimensions 0.5 m x 0.95 m x 0.6 m and the legs are 0.05 m thick in *x*- and *z*- directions. A computer hard drive is placed under the desk and has dimensions of 0.4 m × 0.5 m × 0.2 m. A monitor is placed on the middle of the desk and is 0.15 m × 0.4 m × 0.4 m. A storage box and a mini-refrigerator are placed at the middle of the side wall. The storage box is 0.6 m × 0.8 m × 0.6 m and the mini-refrigerator is represented as a cube with a length of 4 m in each direction. A bookshelf is placed along the opposite wall and has dimensions of 0.22 m × 1.6 m × 0.75 m.

The computer hard drive and monitor have heat dissipation of 70 W and 35 W, respectively [24]. The heat that dissipates from the mini-refrigerator is estimated using the coefficient of performance (COP) and the energy balance equation for the refrigeration system:

$$COP = \frac{Q_{used}}{W_{in}} \tag{29}$$

$$Q_{dissipated} = W_{in} + Q_{used} \tag{30}$$

The estimated energy consumption for a compact refrigerator by Kenmore is 348 kWh/yr, or approximately 40 W [25]. The COP varies from 2.5 to 5. In this study, a COP of 3 is chosen and thus the mini-refrigerator approximately dissipates heat of 120 W. For each device, the heat dissipation normally occurs at the back of the device; thus, the heat flux is applied at the back of each device. No-slip and adiabatic boundary conditions are applied to

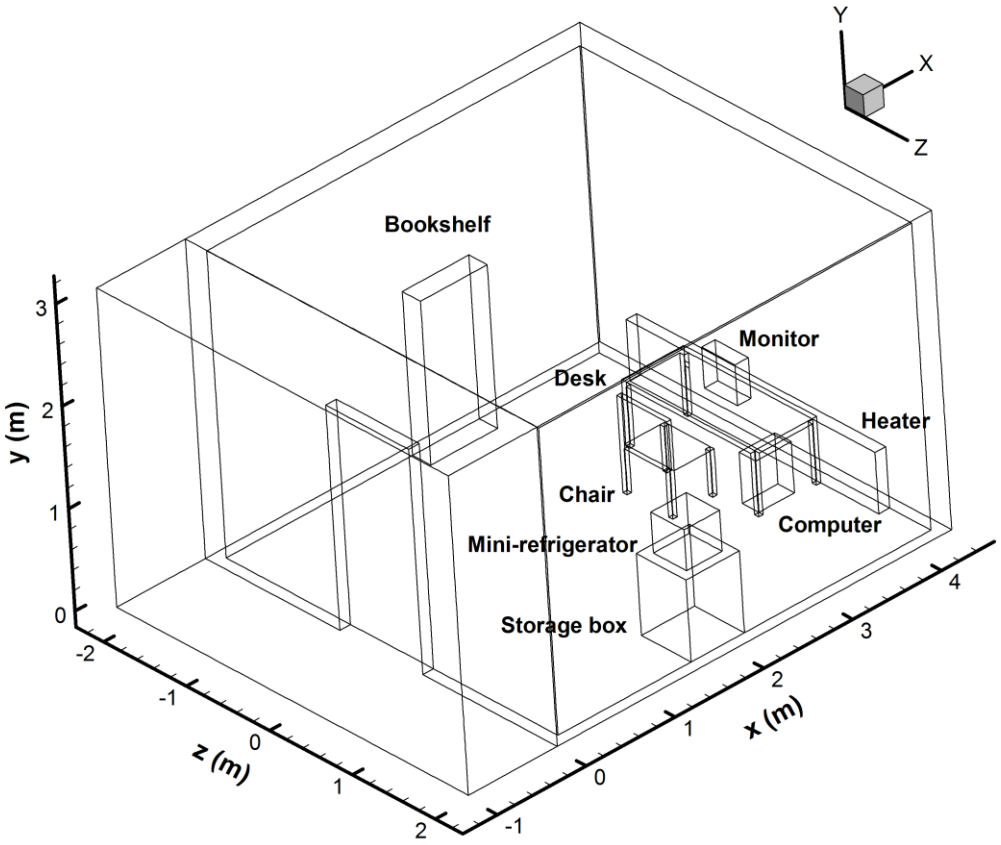

Figure 4.10 Layout of furniture and heat sources in the room

the walls. The heater is also turned on to produce warm air at 50 °C. Domain B (3D) is used, and the simulation with furniture is compared to the case with only a heater (original).

First, the effects of additional heat sources and objects in the room at ambient temperature of 22 °C are discussed. Then using only the furniture case, the effect of ambient condition is studied comparing two ambient temperatures, 22 °C and 10 °C. Lastly, a constant wind of 5 m/s is considered at the left boundary of the domain to study the effect of wind. The units for velocity and pressure in the results are in m/s and Pa, respectively.

4.5.1 Indoor air quality (IAQ) guidelines

Thermal comfort is determined by various factors. For the current study, only two factors are considered: air temperature and velocity. Two ambient temperatures are tested for the following 3D simulations, 22 °C and 10 °C. The recommended indoor temperatures by ASHRAE guidelines [8] changes according to ambient temperature. For T_∞ = 22 °C, the maximum recommended temperature is 25 °C, and the maximum acceptable temperature is 28 °C. For T_∞ = 10 °C, the maximum recommended and acceptable temperatures are 23 and 25 °C, respectively. The minimum indoor temperature for T_∞ = 10 °C is 17 °C.

Air velocity is also an important factor that determines level of indoor thermal comfort. According to ASHRAE guidelines, the maximum acceptable velocity is 0.8 m/s when T_∞ > 25.5 °C and the maximum acceptable velocity is 0.15 m/s when T_∞ < 22 °C. For ambient conditions between 22 °C and 25.5 °C, the maximum velocity allowed is determined by:

$$v_{maximum} = 50.45 - 4.4047\,T_\infty + 0.096425\,T_\infty^2 \tag{31}$$

The recommended conditions by ASHRAE guidelines for two ambient conditions, 22 °C and 10 °C, are summarized in Table 4.3.

Table 4.3 Recommended thermal conditions by ASHRAE guidelines [8].). Used under fair use, 2013

	T_∞ = **22 °C**	T_∞ = **10 °C**
Recommended temperature (°C)	22~25	19~23
Acceptable temperature (°C)	21~28	17~25
Maximum acceptable velocity (m/s)	0.21	0.15

4.5.2 The effects of additional furniture and heat sources in a room

The effects of additional heat sources and objects in the room are studied in this section. Two cases are compared using an ambient temperature of 22 °C: A room with a heater only (original case) and with additional heat sources and furniture.

Temperature contour with streamlines superimposed at t = 2 minutes for the furniture case is shown in Figure 4.11 and compared to the original case in Figure 3.8. Similarly, the ambient air enters the room through the bottom section of the doorway, and then is heated. The heated air rises and then exits through the doorway. The effect of additional heat sources is difficult to observe in the 3D view (Figure 4.11). Therefore, contours at various planes are

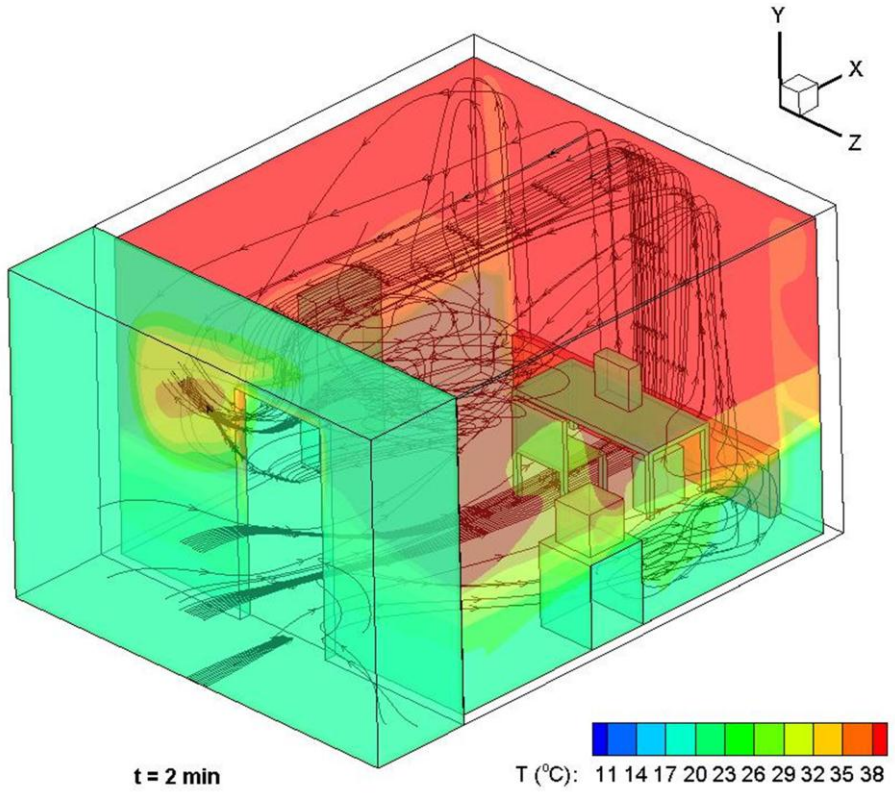

Figure 4.11 Temperature contour with streamline superimposed in 3D at t = 2 minutes for the furniture case with T_∞ = 22 °C

shown in Figure 4.12 to Figure 4.15.

Figure 4.12 (a), (b), and (c) compare *y*-velocity, *x*-velocity, and temperature contours in the *y*-*z* plane at the doorway ($x = 0$ m) for the original case (top figures) and for the furniture case (bottom figures), respectively. Solutions are symmetric for the original case due to the symmetric layout in the room, whereas the solutions with furniture are not symmetric. The largest *y*-velocity occurs approximately at $y = 1.7$ m for each case at the doorway. Examining the *x*-velocity contours, the ambient air enters the room faster for original case than furniture case despite additional heat sources for the furniture case. Temperatures are more uniformly stratified for the original case at the doorway.

Figure 4.13 shows *y*-velocity and temperature contours in the *y*-*z* plane at $x = 1.8$ m, which cuts through the mini-refrigerator and the box. Positive *y*-velocity is visible at the bottom corners for the original case. Similarly, positive velocities occur in front of the storage box since that region protrudes from the wall. At $y = 2.5$ m near the walls, negative *y*-velocity occurs for each case, where the magnitude is larger for the furniture case. Temperature contours for the original and furniture cases are similar, except high temperature is noticeable at the back of the mini-refrigerator due to heat dissipation.

The contours in the *x*-*y* plane at $z = 0$ m and $z = 0.65$ m are plotted in Figure 4.14 and Figure 4.15, respectively. The former and latter planes cut through the computer monitor and computer hard drive, respectively. The pressure contours are shown in the left figures and temperature contours with streamlines superimposed are shown in the right figures.

Examining the plane at $z = 0$ m (Figure 4.14), pressure is high at the top corners of the room for each case, especially above the heater. The original case has larger negative pressure, which occurs at the top of the doorway. Airflow patterns (streamlines) are presented

in Figure 4.14 (b). For both cases, the ambient air enters the room, is heated (mostly by the heater), rises and exits through the doorway. As mentioned in section 0, there is one circulation zone for the original case in the plane at z = 0 m. In contrast, there are two circulation zones for the furniture case; one between y = 2 m and 2.5 m, similar to the 2D results (refer to streamlines in Figure 3.6) and the other behind the chair. Additional furniture in the room affected the airflow patterns, which caused another circulation zone before the chair. The effect of heat transfer from the monitor is insignificant on temperature distribution since only 35 W of heat is dissipated.

Examining the results at z = 0.65 m, high pressure is again noticeable at the top corners in Figure 4.15 (a). In addition, negative pressure is bigger for the original case. A big circulation zone occurs from y = 1.5 m to 2.5 m for both cases (see Figure 4.15 (b)). Three small circulations occur below the big circulation zone for the original case whereas two circulation zones develop below the big circulation zone for the furniture case. High temperatures are noticeable behind the computer and under the desk in Figure 4.15 (b) due to 70 W of heat transfer from the computer.

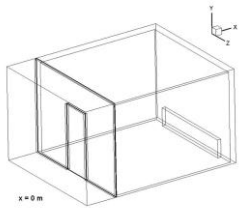

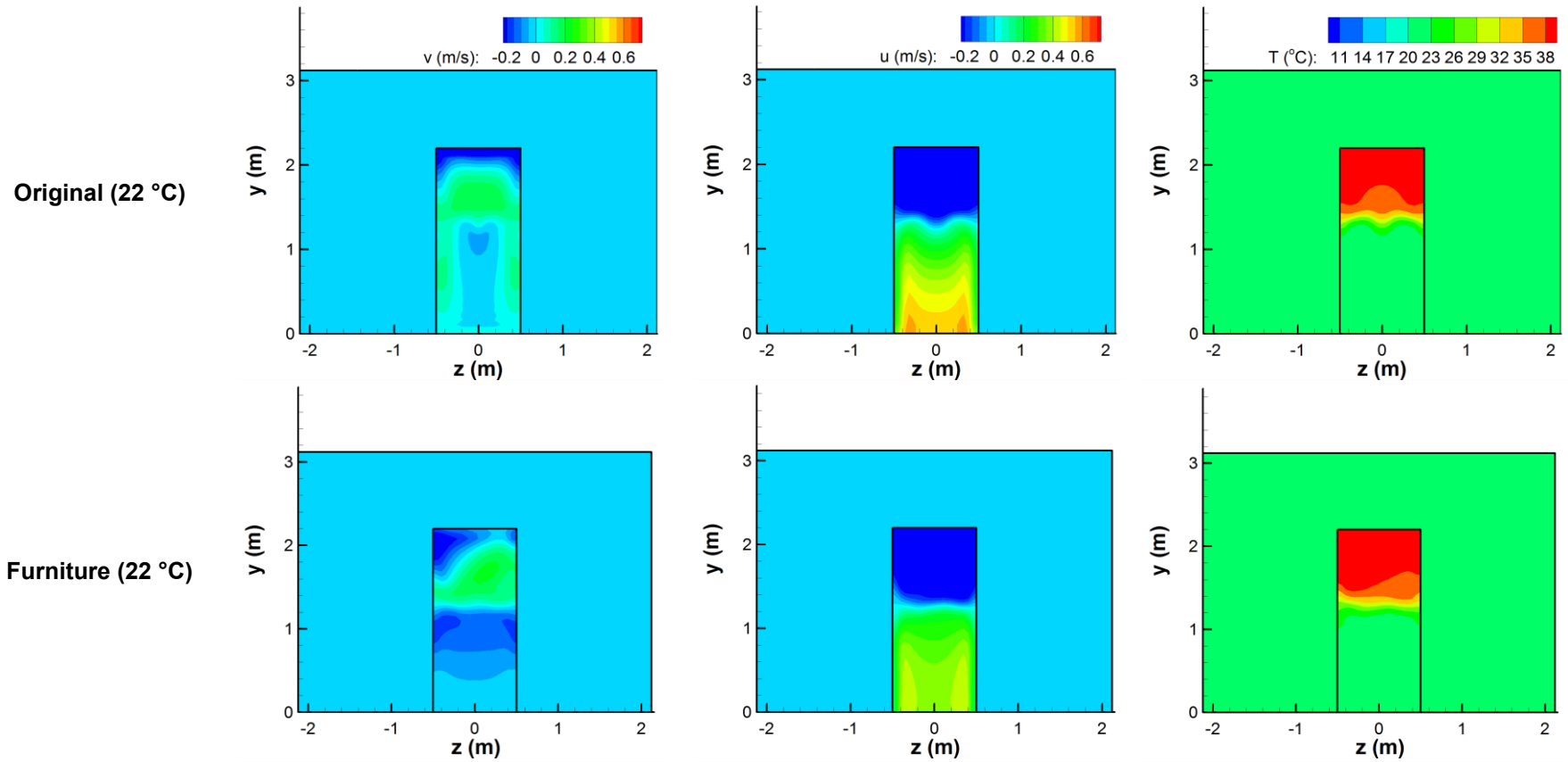

Figure 4.12 Contours in *y-z* plane at the doorway for original (top) and furniture (bottom) cases for T_∞ = 22 °C and u_∞ = 0 m/s: (a) *y*-velocity and (b) temperature

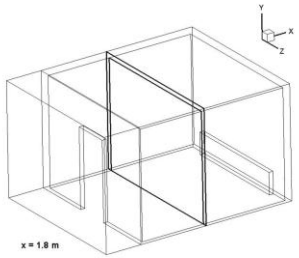

(a) *y*-velocity **(b) Temperature**

Original (22 °C)

Furniture (22 °C)

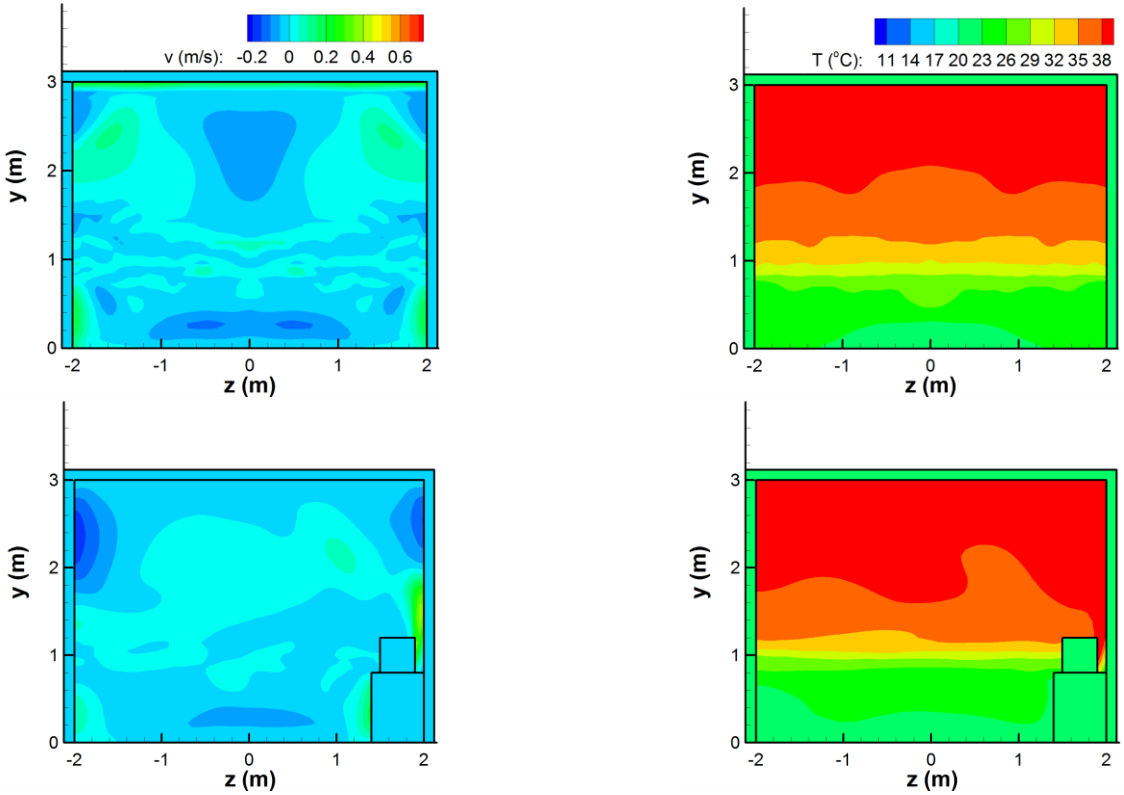

Figure 4.13 Contours in *y*-*z* plane at x = 1.8 m for original (top) and furniture (bottom) cases for T_∞ = 22 °C and u_∞ = 0 m/s: (a) *y*-velocity and (b) temperature

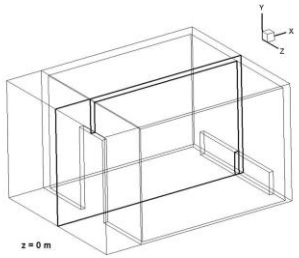

(a) Pressure **(b) Temperature with streamlines**

Original (22 °C)

Furniture (22 °C)

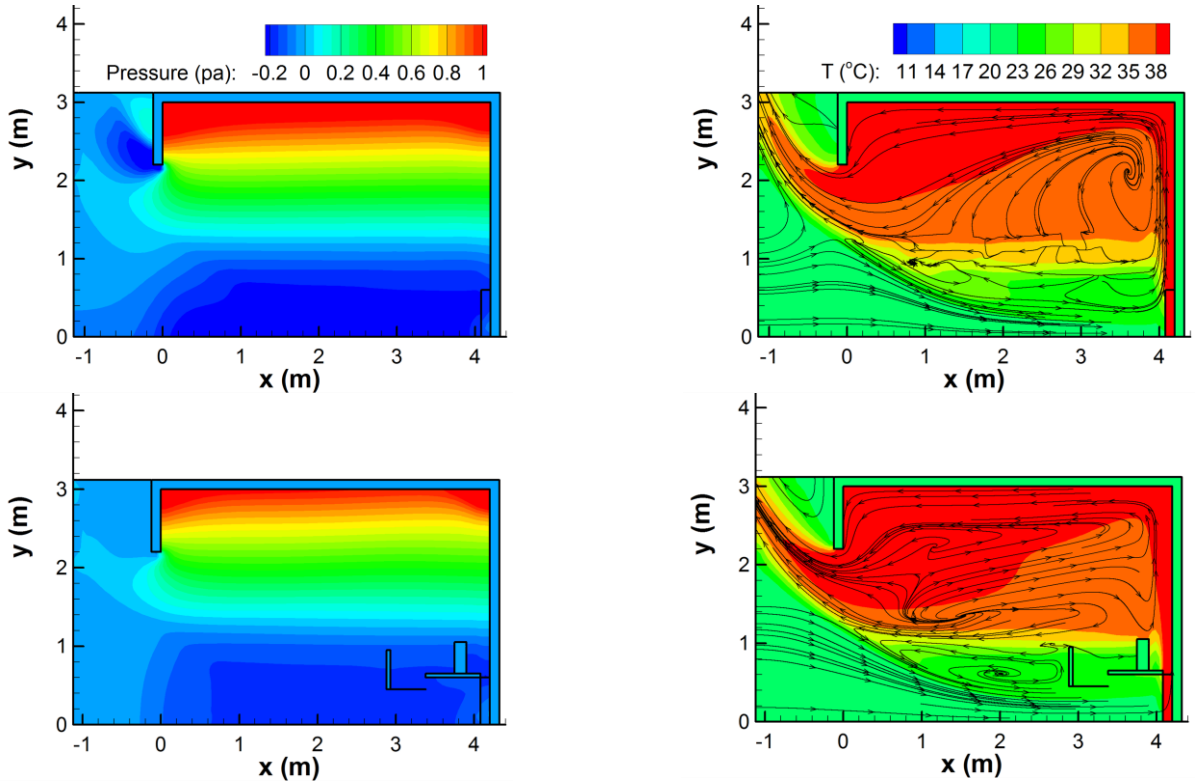

Figure 4.14 Contours in *x*-*y* plane at *z* = 0 m for original (top) and furniture (bottom) cases for T_∞ = 22 °C and u_∞ = 0 m/s: (a) pressure and (b) temperature with streamlines

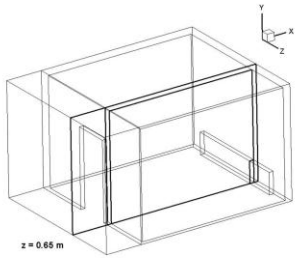

(a) Pressure **(b) Temperature with streamlines**

Original (22 °C)

Furniture (22 °C)

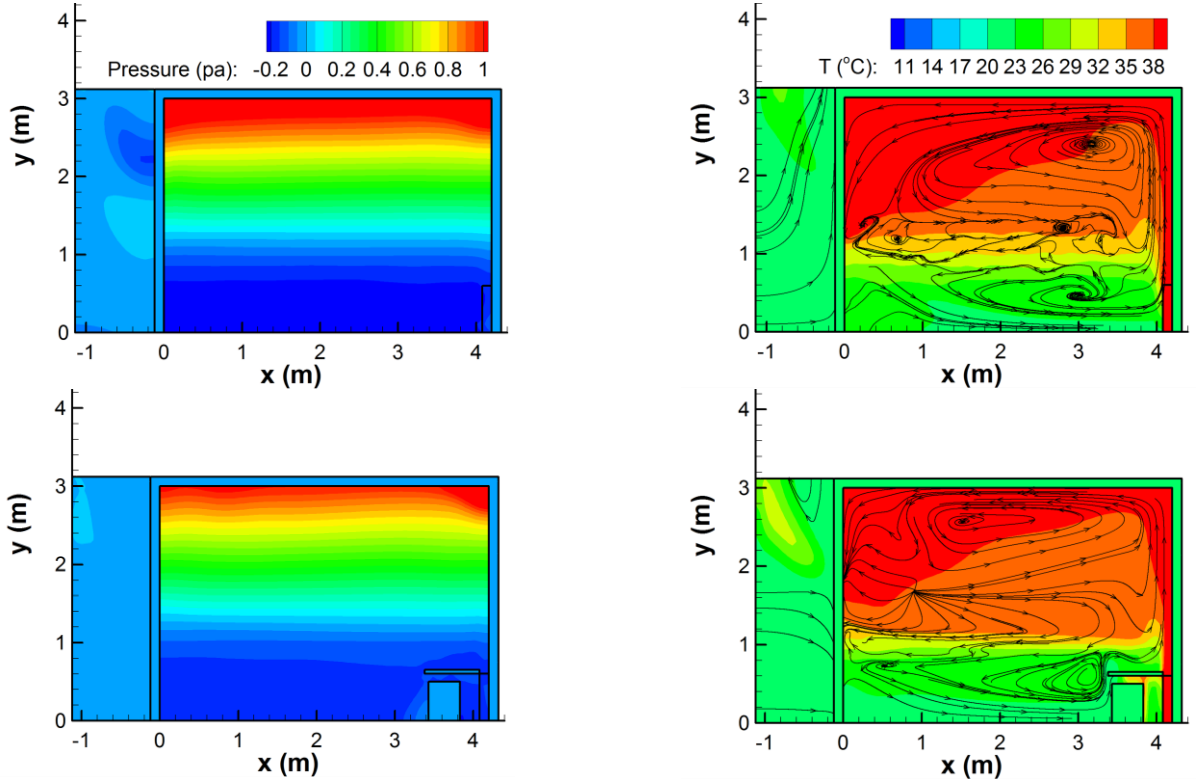

Figure 4.15 Contours in *x*-*y* plane at *z* = 0.65 m for original (top) and furniture (bottom) cases for T_∞ = 22 °C and u_∞ = 0 m/s: (a) pressure and (b) temperature with streamlines

Figure 4.16 shows spatially averaged velocity and temperature along the planes at y = 1 m and 1.5 m for the original and the furniture cases for 3 minutes. Average velocity at each height is larger for the original case than for the furniture case because furniture impedes the motion of the air, slowing down the fluid velocity. Average velocity at y = 1.5 m is larger compared to that at y = 1 m since density of air is lighter due to higher temperature. Average velocity for both cases at each height does not exceed 0.21 m/s, the maximum acceptable velocity by ASHRAE guidelines [8]. Examining Figure 4.16 (b), average temperature at 1 m is higher for the original case than for the furniture case. Similarly, average temperature for the original case is higher than for the furniture case at y = 1.5 m until t = 120 s, but the average temperature for the furniture case becomes higher than for the original case after t = 120 s. The average temperature plot shows that the room at both y = 1 m and 1.5 m reaches 25 ℃, the maximum recommended temperature by ASHRAE guidelines, after the heater is turned on approximately for 15 s. The temperature at y = 1 m and 1.5 m reaches the maximum acceptable value after the heater is turned on approximately for 90 s and 45 s, respectively.

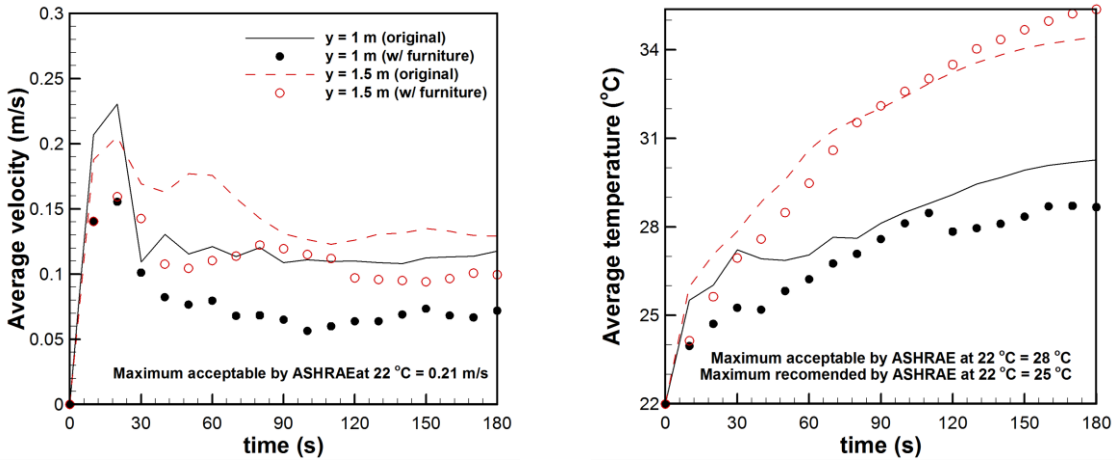

(a) Spatially averaged velocity **(b) Spatially averaged temperature**

Figure 4.16 (a) Spatially averaged velocity and (b) temperature over the planes at y = 1 m and 1.5 m for the original and the furniture cases with T_∞ = 22 °C and u_∞ = 0 m/s

4.5.3 Furniture case: different ambient conditions

4.5.3.1 Ambient temperature of 10 °C

Schaelin et al. [1] modeled a room with a heater for a warm ambient temperature of 22 ℃, which was considered in Sections 3.3 and 0 (the original case). Realistically however, a heater is not usually turned on for such warm air temperatures. In section 4.3, three different ambient temperatures, 22 ℃, 18 ℃, and 14 ℃, were considered in 2D to study the effect of ambient temperatures. In the current section, the 3D room is modeled with furniture at an ambient condition of 10 ℃, which is a more realistic condition for the heater to be turned on.

Figure 4.17 shows temperature contours with streamlines superimposed in 3D for T_∞ = 10 ℃. The room is much cooler compared to the case with T_∞ = 22 ℃ (refer to Figure 4.11). The streamlines show that the heated air exiting through the doorway does not significantly

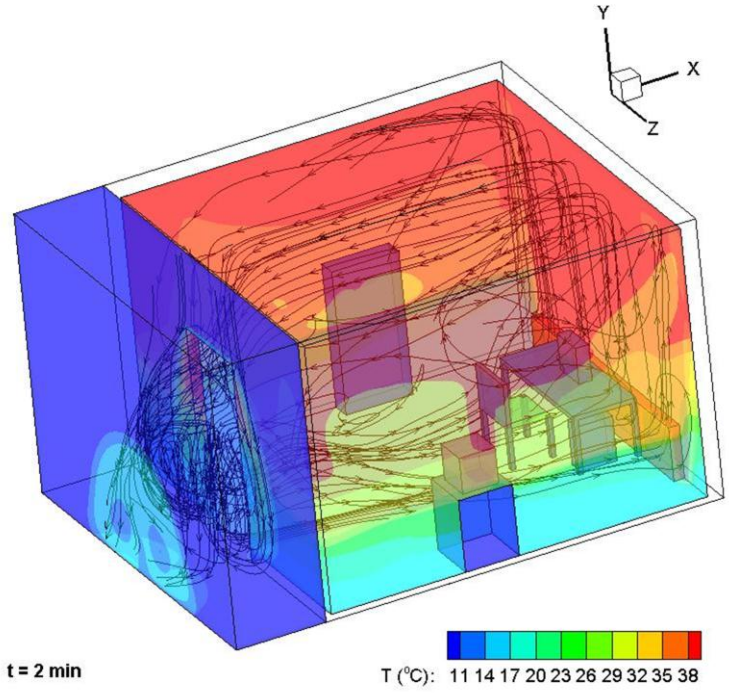

Figure 4.17 Temperature contour with streamline superimposed in 3D at t = 2 minutes for the furniture case with T_∞ = 10 °C and u_∞ = 0 m/s

rise at T_∞ = 10 ℃ as it did for the case with T_∞ = 22 ℃.

The following figures present 2D contours for the furniture case with ambient temperature of 10 °C, which are compared to results for the furniture case at ambient temperature of 22 °C presented in the previous section (refer to the right column of Figure 4.12, Figure 4.13, Figure 4.14, and Figure 4.15). Figure 4.18 (a), (b), and (c) show *y*-velocity, *x*-velocity and temperature contours in the *y*-*z* plane at the doorway, respectively. Similar to the results for the furniture case at T_∞ = 22 °C (refer to Figure 4.12), the solutions are non-

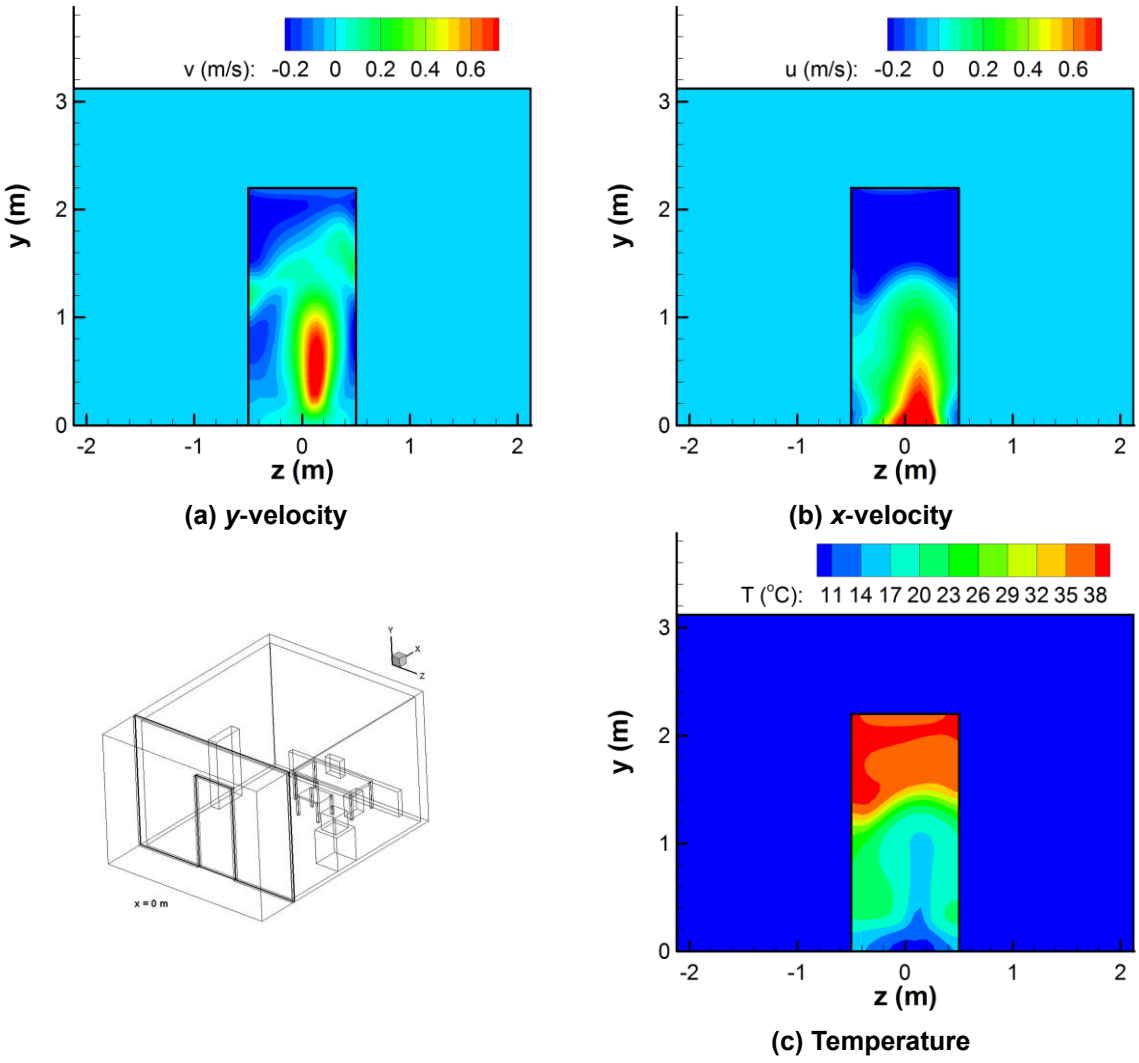

(a) *y*-velocity

(b) *x*-velocity

(c) Temperature

Figure 4.18 Contours in *y*-*z* plane at the doorway for furniture case with T_∞ = 10 °C and u_∞ = 0 m/s: (a) *y*-velocity (b) *x*-velocity and (c) temperature

symmetric. Examining Figure 4.18 (a), the largest y-velocity occurs approximately at y = 0.5 m, whereas it occurs at 1.7 m for T_∞ = 22 °C (refer to Figure 4.12 (a)). Peak velocities are much larger for T_∞ = 10 °C at the doorway compared to T_∞ = 22 °C. Comparing Figure 4.18 (b) to Figure 4.12 (b), the ambient air enters the room faster, and the heated air exits the room slower when T_∞ = 10 °C. The air enters and exits the room evenly throughout the width of the door for T_∞ = 22 °C, while inflow air is concentrated at the middle of the doorway for T_∞ = 10 °C. Due to low ambient temperature, the temperature at the doorway in Figure 4.18 (c) is lower.

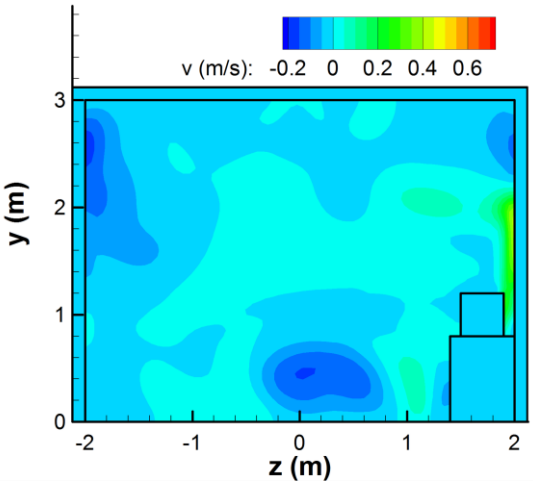

(a) *y*-velocity

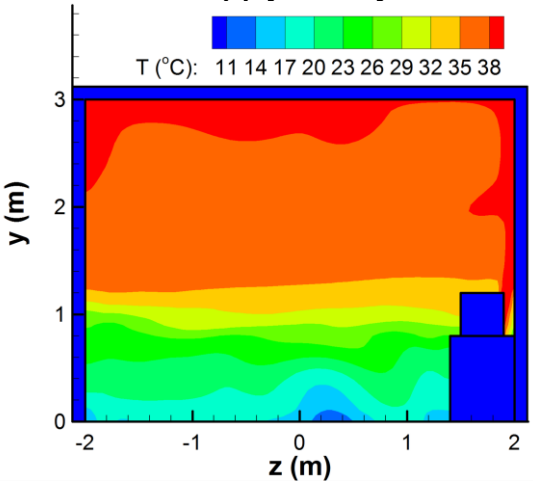

(b) Temperature

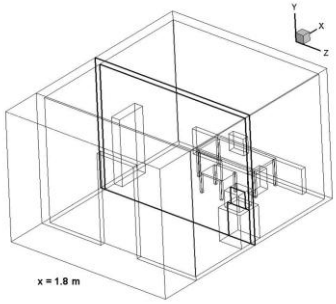

Figure 4.19 Contours in *y-z* plane at *x* = 1.8 m for furniture case with T_∞ = 10 °C and u_∞ = 0 m/s: (a) *y*-velocity and (b) temperature

Figure 4.19 shows *y*-velocity and temperature contours in the *y*-*z* plane that cuts through the mini-refrigerator and the box for T_∞ = 10 ℃ (compared to right column of Figure 4.13). Large velocities and temperatures are noticeable behind the mini-refrigerator due to heat dissipation. There are negative *y*-velocity zones at both side walls, and also in the middle of the plane.

The temperature contours with streamlines superimposed in the *x*-*y* plane at *z* = 0 m and *z* = 0.65 m are plotted in Figure 4.20 (a) and (b), respectively. As discussed, the heated air exits through the doorway, but does not significantly rise at T_∞ = 10 ℃ (Figure 4.20 (a)) as it did at T_∞ = 22 ℃ (refer to right column of Figure 4.14 (b)). The effect of the computer is noticeable below the desk shown in Figure 4.20 (b) while the effect of the monitor is insignificant

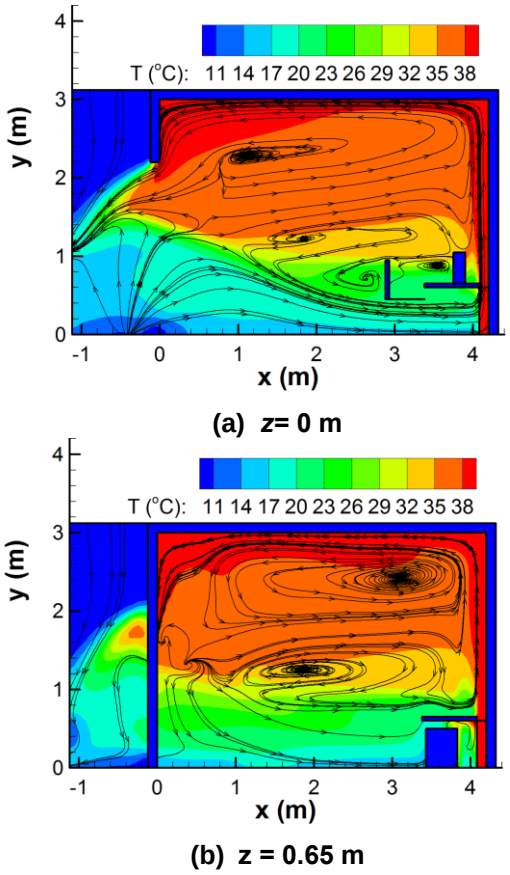

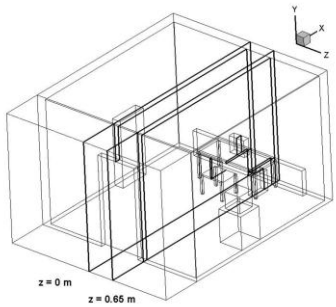

Figure 4.20 Temperature contours with streamlines superimposed in *x*-*y* plane at (a) *z* = 0 m and (b) z = 0.65 m for furniture case with T_∞ = 10 °C and u_∞ = 0 m/s

shown in Figure 4.20 (a). At the plane z = 0 m in Figure 4.20 (a), one additional circulation zone develops in front of the monitor at T_∞ = 10 ℃ compared to the case at T_∞ = 22 ℃ (Figure 4.14). At the plane z = 0.65 m in Figure 4.20 (b), two big circulation zones develop whereas there were multiple circulation zones below the big circulation zone for the furniture case at T_∞ = 22 ℃ (refer to Figure 4.15).

Figure 4.21 shows spatially-averaged velocity and temperature along the planes at y = 1 m and 1.5 m for the furniture case at T_∞ = 10 ℃ and 22 ℃ for 3 minutes. The overall average velocity for T_∞ = 10 ℃ is about twice as large as that for T_∞ = 22 ℃, and approximately 0.1 m/s faster than the recommended air velocity by ASHRAE when T_∞ < 22 ℃ (0.15 m/s). Average velocities for T_∞ = 10 ℃ at y =1 m and 1.5 m are approximately 0.2 m/s and 0.25 m/s, respectively. The average temperature at y = 1 m and 1.5 m for T_∞ = 10 ℃ reaches the recommended temperature (23 ℃) by ASHRAE after 90 s and 60 s, respectively. The maximum acceptable temperature (25 ℃) is reached after 110 s and 90 s at height of 1 m and 1.5 m, respectively, which is not desirable for comfortable conditions.

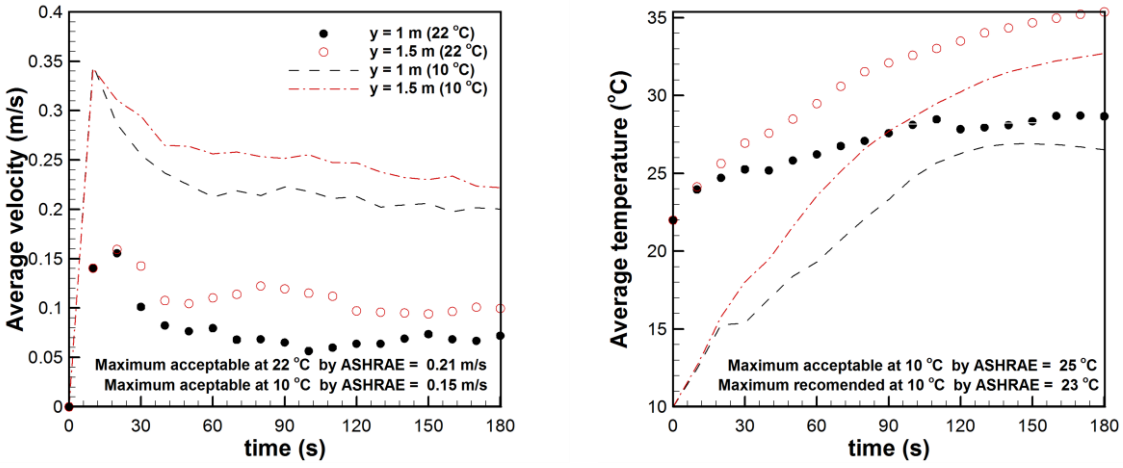

(a) Spatially averaged velocity **(b) Spatially averaged temperature**

Figure 4.21 (a) Spatially averaged velocity and (b) temperature over the planes at y = 1 m and 1.5 m for the furniture case at T_∞ = 10 °C and 22 °C

4.5.3.2 Ambient conditions of 10 °C and 5 m/s

The effect of wind speeds was modeled using 2D simulations in section 4.4. In the current section, wind is modeled in 3D. In addition to the ambient condition of T_∞ = 10 °C, constant wind speed of u_∞ = 5 m/s is applied at the left boundary, parallel to the doorway. The furniture case is modeled and the results are compared to the case without wind at the same ambient condition of T_∞ = 10 °C.

Temperature contours with streamlines superimposed at t = 2 minutes are presented in Figure 4.22. Compared to the case without wind (refer to Figure 4.17), the room is much cooler. Streamlines show that the ambient air enters the room, smoothly circulates out through the doorway, and rises. To better understand airflow patterns and temperature in the

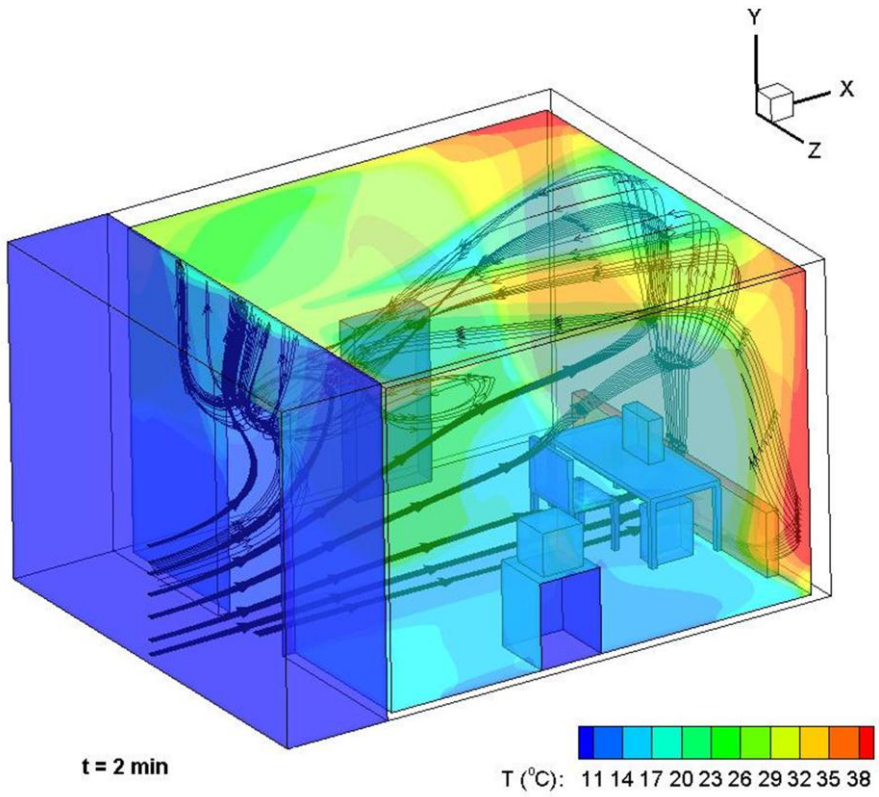

Figure 4.22 Temperature contour with streamline superimposed in 3D at t = 2 minutes for the furniture case with T_∞ = 10 °C and u_∞ = 5 m/s

room, 2D contours are studied in the following figures.

Figure 4.23 shows *y*-velocity, x-velocity, temperature contours at the doorway for the furniture case with T_∞ = 10 °C and u_∞ = 5 m/s. The scales for *x*- and *y*-velocity are different from previous cases (without wind) since the magnitudes are incomparable with velocities from cases without wind. It is noticeable that the magnitude of the *x*- and *y*-velocity is much larger compared to the case without the wind (refer to Figure 4.18). The maximum *y*-velocity occurs approximately at *y* = 2 m, where the magnitude is close to 2.8 m/s. An almost

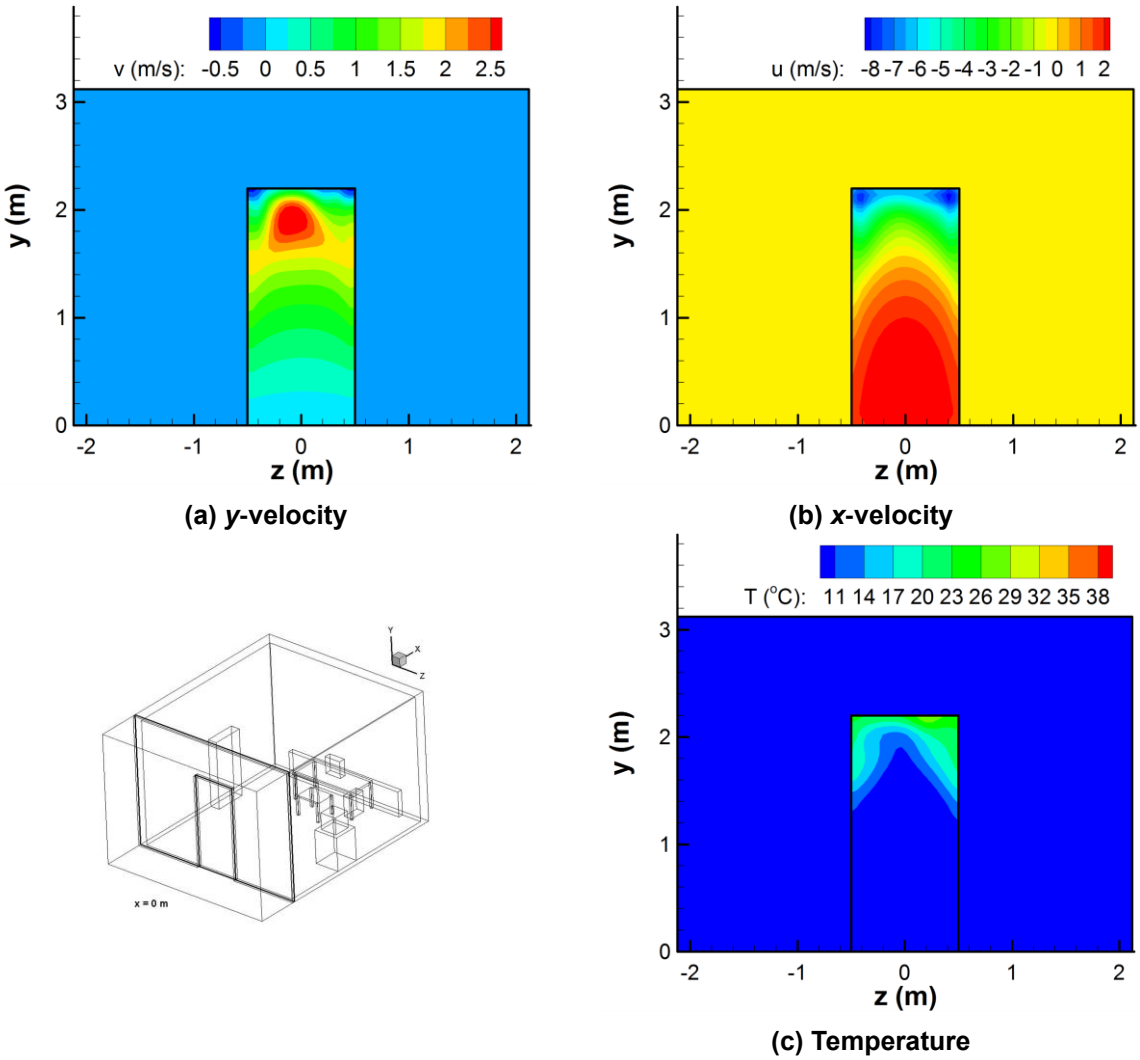

Figure 4.23 Contours in *y-z* plane at the doorway for furniture case for T_∞ = 10 °C and u_∞ = 5 m/s: (a) *y*-velocity and (b) x-velocity (c) temperature

symmetric solution is visible in Figure 4.23 (b). The heated air exiting the room has a larger velocity compared to the ambient air entering the room. Temperature at the doorway is mostly at ambient condition.

Figure 4.24 shows *y*-velocity and temperature contours at the plane that cuts through the mini-refrigerator. The effect of mini-refrigerator is shown, where large *y*-velocity and high temperature are noticeable at the back of mini-refrigerator. Large positive *y*-velocity is also visible at the center of the plane in Figure 4.24 (a). Large negative *y*-velocity zones are

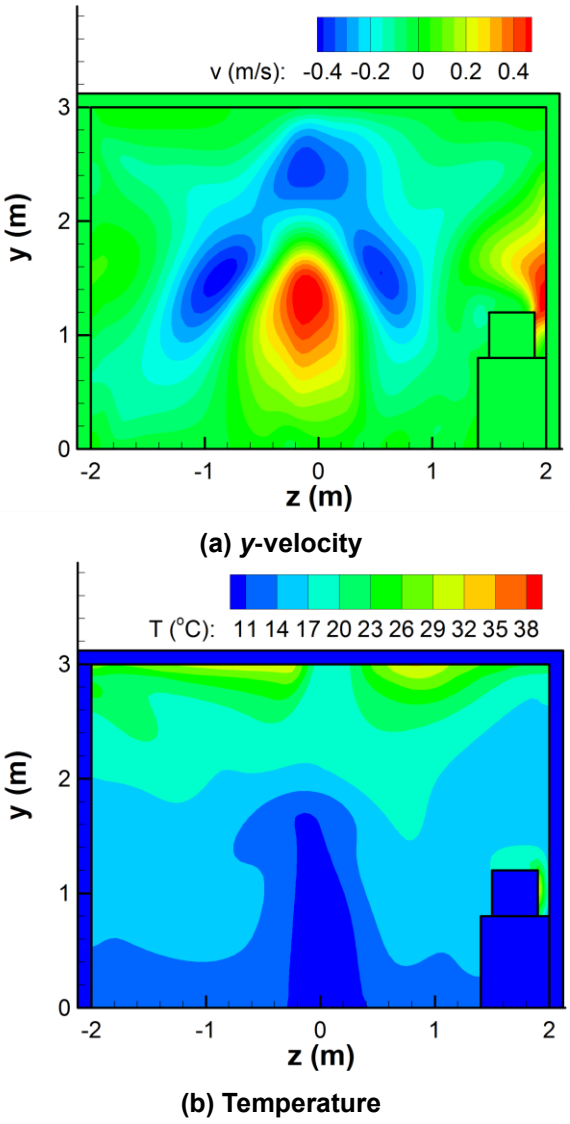

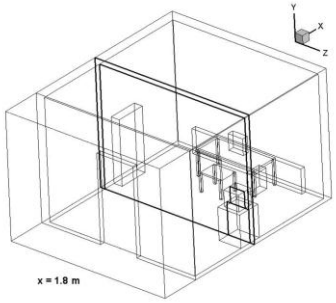

Figure 4.24 Contours in *y*-*z* plane at x = 1.8 m for furniture case for T_∞ = 10 °C and u_∞ = 5 m/s: (a) *y*-velocity and (b) temperature

noticeable surrounding the positive velocity zone at the center. Examining temperature contour, overall temperature at the plane is lower compared to the case without wind (refer to Figure 4.19 (b)).

Figure 4.25 (a) and (b) show temperature contours with streamlines superimposed in *x*-*y* plane at z = 0 m and z = 0.65 m, respectively. The overall temperature in the room is lower compared to the case without wind (refer to Figure 4.20). At both planes, one big circulation zone develops above the desk near the ceiling. Re-examining streamlines in Figure 4.20, multiple circulation zones were observed at z = 0 m, and two big circulation zones at z = 0.65 m. For the wind case, an additional circulation zone develops above the monitor at z = 0 m in

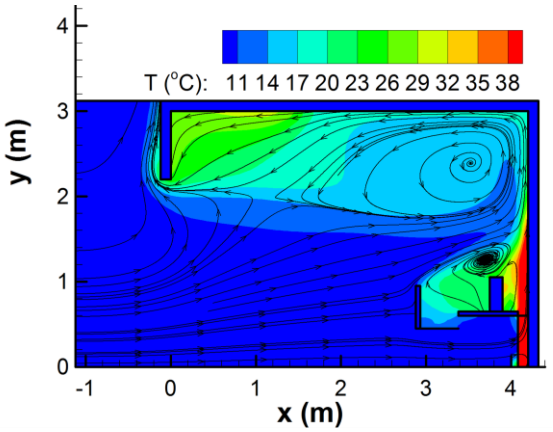

(a) z = 0 m

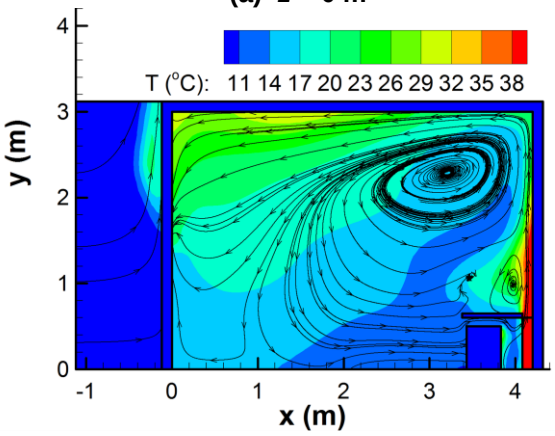

(b) z = 0.65 m

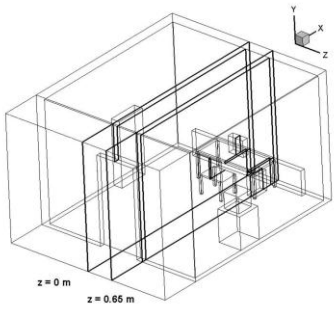

Figure 4.25 Temperature contours with streamline superimposed in x-*y* plane at (a) *z* = 0 m and (b) z = 0.65 m for furniture case with T_∞ = 10 °C and u_∞ = 5 m/s

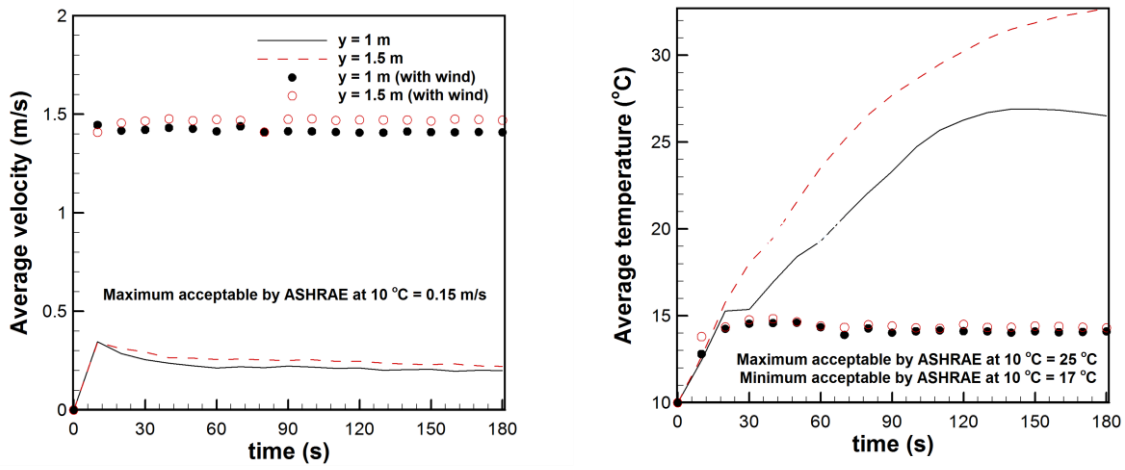

(a) Spatially averaged velocity **(b) Spatially averaged temperature**

Figure 4.26 (a) Spatially averaged velocity and (b) temperature over the planes at *y* = 1 m and 1.5 m for the furniture case at T_∞ = 10 °C without and with wind of 5 m/s

Figure 4.25 (a), and one small circulation zone above the desk at z = 0.65 m in Figure 4.25 (b). High temperature occurs behind each source (monitor and computer) due to heat dissipation.

Spatially averaged velocity and temperature for 3 minutes at heights of 1 m and 1.5 m are shown in Figure 4.26 (a) and (b), respectively. The furniture cases at T_∞ = 10 °C with and without wind are compared. In Figure 4.26 (a), it is noticeable that average velocity for the case with wind is much larger compared to without wind. The velocity is well over the maximum acceptable velocity by ASHRAE guidelines, and is constant with a magnitude of 1.4 m/s. The average temperature at each height is as low as 14 °C, not able to achieve even the minimum temperature recommended (17 °C) by ASHRAE. With T_∞ = 10 °C and u_∞ = 5 m/s, the room is at uncomfortable conditions considering both velocity and temperature.

Chapter 5: Conclusions and Recommendations

5.1 Conclusions

Natural ventilation is a useful method to save energy consumed in buildings mostly for heating and cooling purposes. Since natural ventilation does not depend on a mechanical ventilating system, the ambient conditions (temperature, wind, etc.) and interior spatial layouts are important factors to consider for designing natural ventilating buildings.

A single room with a door was analyzed using computational fluid dynamics. The predictions for velocity and temperature profiles at the doorway were initially validated with the experiments and numerical solutions presented by Mahajan [2] and Schaelin et al. [1], respectively. The current study used 2D and 3D simulations to model three different domains: Domain A, B and C. Domain A included the room and a large ambient environment surrounding the room. Domain B reduced the ambient environment to a small region adjacent to the door opening. Domain C did not include the ambient environment except through boundary condition applied at the door opening. Domain A was not used for 3D simulations due to excessive CPU requirements.

The neutral level and velocity magnitudes at the doorway were best predicted using the smallest domain (Domain C) for 2D modeling, having an error of 5.6 % compared to Mahajan. Larger velocity magnitudes were predicted modeling single-sided ventilation in 3D compared to the experiment. However, the neutral level was very well predicted, where the error was under 2.4 %. In addition, temperature profiles at the doorway for the 3D (Domain B) simulations agreed well with Schaelin et al. Using the velocity and temperature profiles, the heat transfer rates were calculated at the doorway. It was found that the position of the

neutral level was an important factor that affected the total heat transfer rate through the doorway.

The effects of heat loss through the wall were investigated next using 2D simulations. The heat transfer rate through the wall was calculated, where it was 5.6% of the total heat loss in the room with h = 25 W/m^2·K. However, the airflow and temperature within the room showed no significant changes despite modeling conduction through walls.

The effects of decreasing the ambient temperature from 22 ℃ to 14 ℃ were studied in 2D in an effort to represent cooler days. Similar temperature profiles were predicted and only differed in magnitude. It was found that the neutral level height increased as the ambient temperature decreased, and two neutral levels were found at the doorway at 14 ℃. The heat transfer rates at the doorway were calculated for each ambient temperature and it was found that total heat transfer rate through the doorway increased with decreasing ambient temperatures. The velocity vectors and streamlines in the room showed prominent circulation zones, which increased in size with decreasing ambient temperature.

Three different wind speeds were modeled in 2D: 1m/s, 5 m/s and 10 m/s. Non-dimensional velocity profiles for each case were similar. Non-dimensional temperature profiles showed decreasing peak temperature as wind speed increased. Heat transfer rates at the doorway were calculated. For the case where the wind velocity was 1 m/s, total heat transfer rate was positive, that is, heat transferred into the room. Total heat transfer rate increased with increasing wind speeds. While one circulation zone developed for the no-wind case, two more circulation zones were created for wind speed of 5 m/s and 10 m/s. The heated air was more distributed due to big circulation zones for high wind speeds, but there was not a significant air exchange into and out of the room.

Lastly, the room with furniture was modeled using various ambient conditions in 3D. The effects of additional heat sources and furniture were studied by comparing to the case with only a heater (original) and another with furniture at T_∞ = 22 ℃. High temperatures and large velocities were predicted in the vicinity of the heat sources; however the effect of the monitor was relatively small because it dissipated heat at 35 W. Spatially averaged velocity and temperature at various heights were compared between the original and furniture cases over 3 minutes. For both cases, the average velocity never exceeded the maximum recommended velocity by ASHRAE guidelines [8]. The maximum recommended temperature was very quickly reached because the ambient temperature was 22 ℃. Overall, the solutions did not change significantly despite additional heat sources because the effect of the heater was much greater than other heat sources.

The room with furniture was modeled at a cooler condition, T_∞ = 10 ℃, to study the effect of ambient conditions. Larger velocities and lower temperatures occurred due to the cooler ambient temperature. In addition, the heated air exiting through the doorway did not rise as significantly as that for T_∞ = 22 ℃. Spatially averaged velocity for T_∞ = 10 ℃ was approximately twice as large for T_∞ = 22 ℃. At T_∞ = 10 ℃, the average velocity was higher than the maximum acceptable velocity by ASHRAE guidelines [8]. The room at y = 1 m and 1.5 m was able to achieve the maximum recommended temperature within 3 minutes.

A scenario for wind at 5 m/s was considered simultaneously with the low ambient temperature (T_∞ = 10 ℃) for the furniture case, and was compared to the case without wind at the same ambient temperature. The streamlines showed that the ambient air entered through the doorway more smoothly, and cooled the room faster. The spatially averaged

velocity exceeded the maximum acceptable velocity by ASHRAE guidelines, and average temperature in the room was never able to achieve comfortable conditions.

5.2 Recommendations

CFD is a useful tool to model natural ventilation and has great potential in the building energy industry to conveniently analyze the airflow and heat transfer in buildings. However, much work is needed for better modeling and prediction of realistic flows, especially for turbulent buoyancy flows. Natural ventilating buildings highly depend on weather, which is often unpredictable. Further studies concerning the effects of ambient temperature, wind speed, wind directions, and even moisture are recommended.

Building layouts are also an important factor that influences the air flow. The current study only considered a room with a door, where the door was opened all times even during cool conditions. Realistically, it is unlikely to open the door when the heater is turned on. It is recommended to carefully choose the case that can represent realistic situations, and consider multiple openings to study how each opening affects the airflow in the building. Also additional openings (doors or windows) can be considered to study the cross ventilation in the building.

The current study considered additional heat sources and furniture in the room, and changes only in overall solutions were analyzed, where the difference in overall solutions was insignificant. It is recommended to analyze the local changes due to additional heat sources and furniture in the room.

In addition, solar radiation is an important factor for natural ventilation system, which varies during the day and each season. The current study has not considered solar radiation,

but it is recommended to model naturally ventilating buildings considering solar radiation for the future work.

References

[1] Schaelin A., Moser A., van der Maas J. (1992). Simulation of airflow through large openings in buildings. ASHARE Transactions 98 (2):319 - 328

[2] Mahajan BM (1987). Measurement of interzonal heat and mass transfer by natural convection. Solar Energy 38 437 - 466

[3] International Energy Agency(1996). World Energy Outlook 1996. 237-285

[4] International Energy Agency(1997). Energy Statistics and Balances.

[5] U.S. Department of Energy(2008). Annual Energy Review 2007. Washington, DC: Energy Information Administration

[6] Emmerich S.J., Axley J.W., Dols W.S. (2001). Natural Ventilation Review and Plan for Design and Analysis Tools. NIST Interagency Report 6781

[7] U.S. Environmetnal Protection Agency(1989). Report to Congress on indoor air quality. Volume 2. Washington, DC

[8] ASHRAE(2010). ASHRAE Standard 55-2010. Thermal Environment Standards for Human Occupancy Atlanta, GA

[9] Awbi H.B Cho YJ(2007). A study of the effect of heat source location in a ventilated room using multiple regression analysis. Building and environment 42 2072-2082

[10] Stoakes P., Battaglia F., Passe U. (2011). Predicting natural ventilation flows in whole buildings. Part 1: The Viipuri Library. Building Simulation 4 263-276

[11] Stoakes P., Battaglia F., Passe U. (2011). Predicting natural ventilation flows in whole buildings. Part 2: The Esherick House. Building Simulation 4 365-377

[12] Ansys Incorporated(2009). 4.4 Standard, RNG, and Realizable k-ε Models.

[13] Chow W.K., Li J. (2007). Numerical simulations on thermal plumes with *k-ε* types of turbulence models. Building and Environment 42 2819-2828

[14] Starakakis G.M., Vrachopoulos M.Gr, Markatos N.C, Koukou M.K. (2008). Natural cross-ventilation in buildings: Building-scale experiments, numerical simulation and thermal comfort evaluation. Energy and Buildings 40 1666-1681

[15] Awbi H.(2003). Ventilation of buildings. 2nd ed. London: Spon Press

[16] Ansys Incorporated(2009). 13.2.4 Natural Convection and Buoyancy-Driven Flows (User's Guide).

[17] Ansys Incorporated(2009). FLUENT 12.0 User's Guide.

[18] A. J. Chorin (1968). Numerical solution of navier-stokes equations. Mathematics of Computation 22 745-762

[19] Ferziger J.H., Peric M. (2002). Computational Methods for Fluid Dynamics. 3rd edition

[20] Wilson D.J., Kiel D.E.(1990). Gravity driven counterflow through an open door in a sealed room. Building and Environment 25 (4):379-388

[21] Roache P. J.(1994). Perspective: A method for uniform reporting of grid refinement studies. International Journal of Heat and Fluid Flow 24 54-66

[22] Richardson L., Gaunt A. (1927). The Deferred Approach to the Limit. Part I. Single Lattic. Part ll. Interpenetrationg Lattices. The Philosophical Transcations of the Royal Society of London Series A, Containing papers of a Mathematical or Physical Character, 116 (3):405-41

[23] van der Mass J.(1992). Air flow through large openings in buildings. Energy Conservation in Buildings and Community Systems Programme Annex 20 Technical Report (Subtask 2 : Air Flows between Zones):

[24] hp invent(2007). QuickSpecs. HP L1908w 19-inch Widescreen LCD Monitor.

[25] Kenmore(2010). Compact refrigerator: 46-94683/9.